Analysis of the memory system in *Dionaea muscipula*

ハエトリソウの記憶機構の解析

Suda, Hiraku

須田　啓

Doctor of Philosophy

The Graduate University for Advanced Studies, SOKENDAI

School of Life Science

Department of Basic Biology

2020

Table of contents

1. General introduction

Plants have systems to memorize stresses from the environments, for example, temperature stimuli, drought stimuli, and wounding stimuli (Crisp et al., 2016). This stimulus information is stored and recalled when plants accept the same stimulus again (Thellier and Lüttge, 2013). Mechanisms of the memory formation are considered as regulations of signaling metabolites or transcription factors, or regulations of gene expressions by the modification of chromatin states (Crisp et al., 2016).

Thigmonasty is a movement that is independent of the direction of the mechanical stimuli and moves in a certain direction. Memory systems in the thigmonasty are known in *Mimosa pudica* and *Dionaea muscipula* (Dionaea) (Gagliano et al., 2014; J. M. Macfarlane, 1892). However, it is difficult to explain the mechanisms of memory systems of the thigmonasty by regulations of metabolites, transcription factors, and chromatin modifications, because memories are formed immediately after the mechanical stimuli in *Mimosa pudica* and Dionaea (Gagliano et al., 2014; Brown and Sharp, 1910).

Mimosa pudica senses mechanical stimuli by its pulvini at the bases of the plant leaves or leaflets, and leaflets and leaves fold. One of the hypothesized mechanisms of the movement is the turgor change. The movement of *Mimosa pudica* is evoked at the motor cells in the pulvini. Cells of extensor halves of the pulvini shrink after the mechanical stimulus, and leaflets and leaves fold. In previous studies, it has been considered that the mechanical stimulus triggers Ca^{2+} releases from the vacuoles where tannin, a type of polyphenol, is deposited (tannin vacuoles) and cell-walls (Toriyama and Jaffe, 1972), then K^+ and Cl^- flow out from cells of the flexor halves of the pulvini to the cells of the extensor halves of the pulvini (Samejima and Sibaoka,

1980; Toriyama, 1955). These ion effluxes reduce cytosolic osmotic pressure, and turgor decrease by osmotic water movement results in changes of cell states from turgid to flaccid and shrinkage of extensor half pulvini (Satter and Galston, 1981). This thigmonastic motion is diminished by the habituation that the response is desensitized by repeated stimuli. Habituation training to the mechanical stimuli by dropping plants from 15 cm height is memorized immediately, and the degree of leaf movements by the mechanical stimuli is decreased for over 1 month (Gagliano et al., 2014).

On the other hand, Dionaea has a different memory system before the thigmonastic motion. Dionaea is a carnivorous plant that catches preys by snap-trap leaves, leaves are closed by two successive mechanical stimuli to the hair-like tissues called sensory hairs on the leaf blades and catch preys. The first stimulus does not trigger the movement, and the second stimulus within approximately 30 seconds triggers the leaf closure (J. M. Macfarlane, 1892; Juniper et al., 1989a; Brown and Sharp, 1910). This result suggests that Dionaea leaves memorize the first mechanical stimulus for approximately 30 seconds.

Previous studies showed that thigmonastic motion in Dionaea is triggered as follows. First, mechanical stimuli are sensed by sensory hairs. Both first and second mechanical stimuli trigger the propagation of action potentials on the leaf blades (Sibaoka, 1991; Burdon-Sanderson and Page, 1876). After the second stimulus, the movement starts. Turgor change at leaf blade cells is considered as the mechanisms of initiation of the prey capture movement as same as the hypothesized mechanism in the *Mimosa pudica* movement (Brown 1916; Poppinga et al. 2013). This hypothesis is supported by the fact that decreased water level of cultivation pots inhibits the leaf closure in Dionaea (Escalante-Perez et al., 2011). In addition, it is known that K^+

absorption is activated at the adaxial side of the snap-trapping leaf blades during a leaf opening state in the *Aldrovanda vesiculosa* which is the closest species of Dionaea (Iijima and Sibaoka, 1983). Other hypothesis has been proposed that H^+-ATPase-derived pH decrease triggers cell wall-loosening, and cells are expanded by turgor pressure of cells (Williams and Bennett, 1982). After movement started, the movement speed is enhanced by shape change of leaf blades from concave to convex, which is caused by the release of elastic energy stored in the opening state leaves (Forterre et al., 2005).

In Dionaea, the locations of mechano-sensitive tissues were identified (Benolken and Jacobson, 1970), and mechano-sensitive tissues and movement tissues are located in different positions on the leaf blade (Forterre et al., 2005; Benolken and Jacobson, 1970). These traits are suitable to analyze spatially separated signal transduction from the mechano-sensing to the movement rather than *Mimosa pudica* where the locations of the mechano-sensitive cells are still under discussion (Hagihara and Toyota, 2020). Although the locations of sensor cells were identified, the molecular mechanisms of the reception of the mechanical stimulus and the intracellular molecular dynamics between the mechanical stimulus and the movement were poorly understood in Dionaea, because the thigmonastic motion finished in less than one second after the second mechanical stimulus (Forterre et al., 2005; Poppinga et al., 2013). Although observation of molecular dynamics in high temporal resolution is difficult without reverse genetics in plants, no transformation method of Dionaea has not been established so far.

In this thesis, I focused on the Dionaea to understand the signal transduction following to the mechanical stimulus, and how Dionaea memorizes mechanical stimulus

and triggers the movement. In previous studies, the only known response after the mechanical stimulus in Dionaea is the induction of action potential, which propagates on the leaf blade (Burdon-Sanderson and Page, 1876). Leaf movement starts after two successive stimuli, both of which trigger action potentials (Sibaoka, 1991). On the other hand, no molecule is known as a mechanical stimulus responsive-factor.

One of the candidates of mechanical stimulus-responsive signal transmitters is Ca^{2+} which is a second messenger in plant signaling and responds to the mechanical stresses (Knight et al., 1992). Recently, genetical imaging methods enabled the visualization of the Ca^{2+} in plants (Vincent et al., 2017).

I established a transformation method of Dionaea, and analyzed spatial-temporal cytosolic Ca^{2+} concentration ($[Ca^{2+}]_{cyt}$) changes in Dionaea using transformant to understand the Ca^{2+} dynamics following to the reception of mechanical stimuli in Dionaea and provide new insights about regulatory mechanisms of the thigmonastic motion in plants.

2. Introduction

The leaves of the carnivorous plant Venus flytrap, *Dionaea muscipula* (Dionaea) close rapidly to capture insect prey. The closure response usually requires two successive mechanical stimuli to sensory hairs on the leaf blade within approximately 30 seconds (J. M. Macfarlane, 1892; Juniper et al., 1989a; Brown and Sharp, 1910; Burri et al., 2020). An unknown biological system in Dionaea is thought to memorize the first stimulus and transduce the signal from the sensory hair to the leaf blade(Juniper et al., 1989a).

In the short-term memory system of Dionaea (Fig. 1a), the second stimulus to any of six sensory hairs can trigger movement (Fig. 1b), regardless of which hair received the first stimulus (Juniper et al., 1989a). Previous studies showed that mechanical stimulation of a sensory hair generates action potentials that propagate to both lobes of the leaf (Benolken and Jacobson, 1970; Sibaoka, 1966). Other studies have shown that leaf closure is blocked by Ca^{2+} channel inhibitors that should inhibit the increase of the cytosolic Ca^{2+} concentration ($[Ca^{2+}]_{cyt}$) of leaf cells, emphasizing the importance of Ca^{2+} in the response (Hodick and Sievers, 1989, 1988; Fagerberg and Allain, 1991). Based on these results, the mechanism of Dionaea memory has been proposed to be as follows (Hodick and Sievers, 1988; Hedrich and Neher, 2018): 1) $[Ca^{2+}]_{cyt}$ increases during excitation; 2) $[Ca^{2+}]_{cyt}$ or the concentration of some Ca^{2+}-activated regulatory molecules must reach a threshold for movement; 3) a single action potential is not enough to increase $[Ca^{2+}]_{cyt}$ to the threshold, and at least two action potentials are necessary to trigger movement; 4) $[Ca^{2+}]_{cyt}$ decreases after the first stimulus, and after 30 s does not reach the threshold even with a second stimulus. This hypothesis has not been directly tested because of the lack of a method for

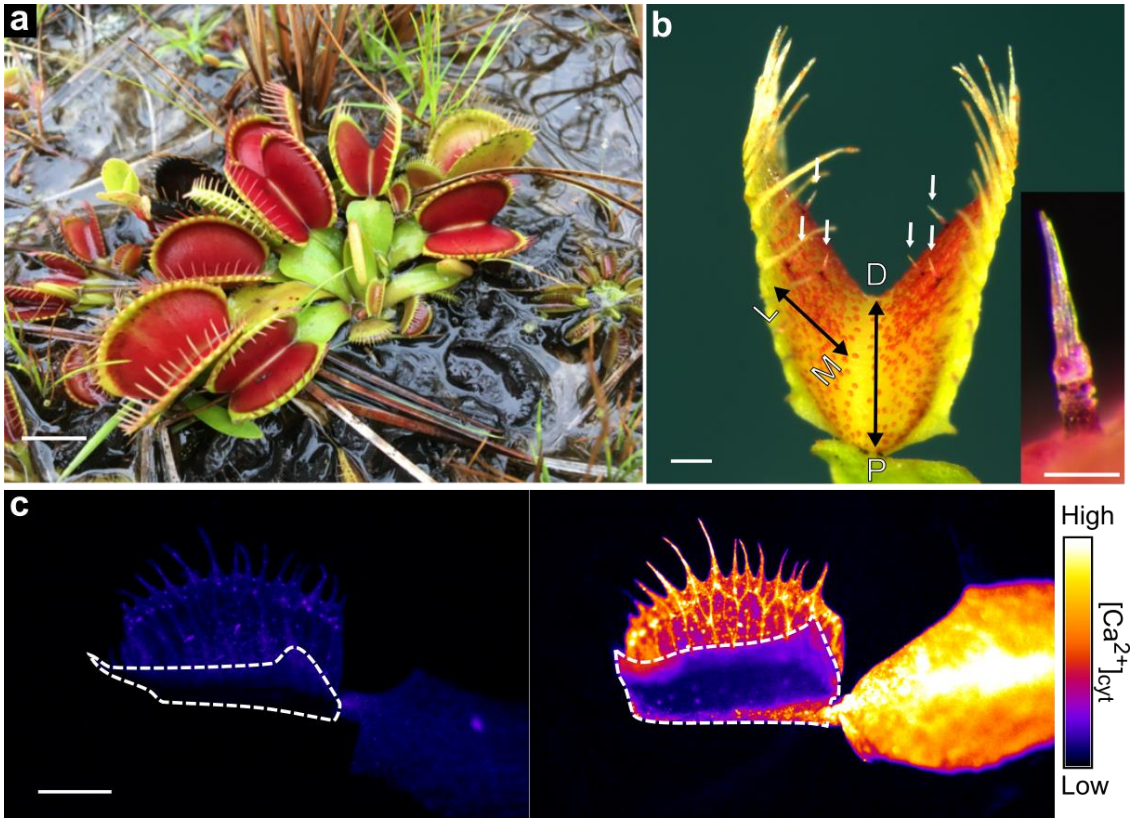

Fig. 1: Cold stimulation induces a $[Ca^{2+}]_{cyt}$ increase in a Dionaea trap leaf.

a, A Dionaea plant growing in its natural habitat, North Carolina, USA. Leaves form a rosette and the bi-lobed leaf blade of each leaf forms a trap.

b, Six sensory hairs (arrows) of a Dionaea leaf, one of which is magnified in the inset. L, lateral direction; M, medial direction; D, distal direction; P, proximal direction.

c, GCaMP6f fluorescence images of a leaf blade before (left) and 2 minutes after (right) a cold stimulus. The abaxial side of a petiole and right half of a leaf blade (a right leaf lobe) were attached to an ice block and cpEGFP signals were detected in cells attached to the ice. The left leaf lobe (outlined by dashed line) did not touch the ice block and the cpEGFP signal was not detected. Immature leaves which do not sense mechanical stimulus and do not propagate calcium signal from the sensory hairs are used in this experiment.

Scale bar, 1 cm in (**a**); 1 mm in (**b**) and (**c**); 100 μm in the inset of (**b**).

spatiotemporal calcium monitoring in Dionaea.

Here, I link signal memory to calcium dynamics using transgenic Dionaea expressing a Ca^{2+} sensor. Stimulation of a sensory hair caused an increase in cytosolic Ca^{2+} concentration ($[Ca^{2+}]_{cyt}$) starting in the sensory hair and spreading to the leaf blade. A second stimulus increased $[Ca^{2+}]_{cyt}$ to an even higher level, meeting a threshold that is correlated to the leaf blade closure. Because $[Ca^{2+}]_{cyt}$ gradually decreased after the first stimulus, the $[Ca^{2+}]_{cyt}$ increase induced by the second stimulus was insufficient to meet the putative threshold for movement after about 30 seconds.

3. Materials and methods

3.1. Plant materials and culture conditions

Seeds of Dionaea were kindly provided by Dr. John Mundy (University of Copenhagen, Denmark) (Jensen et al., 2015), and sterilized in 80% (v/v) EtOH for 1 min, 1% (w/v) benzalkonium chloride for 5 min, and 1% (w/v) sodium hypochlorite for 5 min. The seeds were rinsed three times in water and were sown on the half-strength Murashige and Skoog medium containing 3% (w/v) sucrose, 1× Gamborg's vitamins, 0.1% (w/v) 2-(N-morpholino) ethanesulfonic acid, 0.05% (v/v) Plant Preservative Mixture (Plant Cell Technology) and 0.3% (w/v) Phytagel. The seeds were incubated at 25°C in continuous light until germination. Plants were cultured on modified co-cultivation medium (Mano et al., 2014) (half-strength basal MS salts [1/2 MS; Wako] medium with 2% [w/v] sucrose, 1× Gamborg's vitamins [Sigma-Aldrich], 0.1% [w/v] 2-[Nmorpholino] ethanesulfonic acid [Dojindo Laboratories] at pH 6.1) with 0.3% [w/v] phytagel (Sigma-Aldrich) in a tissue culture vessel (CUL-JAR300; AGC Techno Glass) under continuous light conditions at 25°C. For transformation, Dionaea plants cultivated under continuous light conditions were moved to continuous dark conditions and cultivated from a month to half a year to collect etiolated leaves.

3.2. Transformation

To generate transgenic Dionaea constitutively expressing sGFP or GCaMP6f, the Super-binary acceptor vector pSB1, and the Super-binary intermediate vector pSB11 harboring the *sGFP* or *GCaMP6f* sequence (Chiu et al., 1996; Chen et al., 2013; Komari et al., 2015) were individually introduced into LBA4404 agrobacterium (Hellens et al., 2000). Agrobacteria were cultivated on solid LB medium (Sigma-

Aldrich) Supplemented with 1.5% (w/v) agar (Nacalai Tesque) and 50 μg/ml (w/v) Hygromycin-B (Life Technologies) for 48 h at 30°C. A single agrobacterium colony was inoculated into 5 ml of liquid LB medium with 25 μg/ml (w/v) Hygromycin-B and precultured at 28°C for 24 h with shaking at 180 rpm. Then, a portion of the agrobacteria was diluted to a concentration of OD_{600} = 0.15 with 40 ml of liquid LB medium Supplemented with 25 μg/ml Hygromycin-B in a 200 ml baffled flask, and further cultivated at 28°C with shaking at 180 rpm until an OD_{600} of approximately 0.55 was reached. After centrifugation at 5000×g for 10 min at 25°C, the Supernatant was removed and precipitated agrobacterium cells were resuspended to OD_{600} = 0.3 in the modified co-cultivation medium mentioned above with 40 μg/ml acetosyringone (Wako) after washing with the modified co-cultivation medium once. Etiolated leaves were cut at the middle of the petiole, submerged in 10 ml of the agrobacterium suspension, and placed twice successively under a vacuum (–0.08 MPa) for 10 min. The infected leaves were submerged in the modified co-cultivation medium with fresh agrobacterium, and cultivated under continuous darkness at 25°C for 72 h. Agrobacterium-infected leaves were transplanted onto the modified co-cultivation medium with 0.3% [w/v] phytagel and 150 μg/ml cefotaxime sodium salt (SANOFI), and cultivated under continuous darkness at 25°C. The solid medium was exchanged once a week for at least 1 month, until transgenic shoots formed. One month after infection, the leaves were transferred to solid 1/2 MS medium plates lacking Cefotaxime sodium salt. Transgenic shoots were cultivated under 8 h light / 16 h darkness at 25°C until green leaves formed, and acclimated under 16 h light / 8 h darkness at 22°C in soil consisting of peat moss and perlite at a ratio of 2 to 1.

3.3. Tissue clearing

Leaves were fixed in 20% (v/v) acetic acid (Wako) dissolved in ethanol (Wako) with four 15-min rounds of decompression to 0.08 MPa at room temperature, and then kept overnight at 4°C. Fixed leaves were rehydrated using a dilution series of ethanol (90%, 70%, 50%, 30%, 0%), and cleared in a solution consisting of 8 g chloral hydrate (Wako), 1 ml glycerol (Wako), and 2 ml distilled water for 3 days at room temperature under continuous dark conditions.

3.4. Microscopy

Stereoscopic images and videos were taken using a SZX16 (Olympus) fluorescence microscope equipped with a SZX2-FGFP long-pass filter (Olympus) and a digital camera DP74 (Olympus). Fluorescence videos were taken using the linear mode of cellSens Standard (1.17) in a range where the fluorescence intensities of samples and brightness values of captured images are linear. All fluorescence movies were taken at 50 frames per s, with a 2-ms exposure time (Fig. 5a and b) or 15-ms exposure time (others) and 16× gain, in linear contrast mode, and with 2 × 2 binning. Images were saved as a sequence of uncompressed tiff files. Blue, green, and red channels were split from the original images and only green channel images were used for the analysis. All fluorescence images were pseudocolored with green or LUT (fire lookup table) in ImageJ (1.52p). All movies were constructed from the green channel images of the original uncompressed tiff images. The time course of the two-dimensional propagation of increased fluorescence was determined by manually connecting the boundaries of fluorescent areas (Fig. 5d and e). To calculate the propagation velocity of the $[Ca^{2+}]_{cyt}$ increase, leaves and petioles were considered to be flat planes, and the velocity induced

by the stimulus was measured 0.04 s (Fig. 8a and c), 0.02 s (Fig. 8b) and 5 s (Fig. 8d) after the stimulus. To compare the areas with increased $[Ca^{2+}]_{cyt}$ after application of the first and second stimuli, the pixel intensity distribution was classified into two distributions: pixels with large changes and pixels with small changes in intensity. Pixels with small changes were set as background and were assigned the same value in images acquired after the first and second stimulation. For quantitative analysis, two ROIs (regions of interest) were defined: the central and lateral areas, corresponding to the areas where secondary leaf veins run parallelly and merge with neighboring veins, respectively (Fig. 5h). The size of each ROI was set to at least 1,000 pixels, and the average intensity per pixel in the ROI was calculated using ImageJ, and data were plotted by Microsoft Excel (16.0.12325.20280) and R studio (1.2.1335). Confocal microscope images to evaluate localization of GCaMP6f were taken using a confocal laser microscope SP8 (Leica) with a detecting fluorescence emission of 491-534 nm for cpEGFP or 670-700 nm for auto fluorescence of chroloplast under excitation at 484 nm.

3.5. Image and regression analyses

To quantify the fluorescence intensity using multiple leaves, the fluorescence intensity was calculated at a given time "t" as $F_t = (f_t – f_0) / (f_1 – f_0)$, where f_t indicates fluorescence intensity at a given time "t", f_0 indicates an average of f_t in 50 frames for 1 s before the first stimulus was applied, and f_1 indicates the maximum f_t after the first stimulus was applied before the second stimulus was applied (Fig. 12a and Fig. 13). For the explanatory variables of the regression analysis, the maximum F_t after the second stimulus was defined as F_{max}, the residual F_t immediately before the second stimulus was applied was defined as F_{res}, and duration between times of f_1 and the second

stimulus. As the dependent variables, closed and unclosed leaves after the second stimulus were scored as 1 and 0, respectively. For the likelihood ratio test, I set a null hypothesis that leaf movement is independent of F_{res} or F_{max} and an alternative hypothesis that leaf movement is dependent of F_{res} or F_{max}, and tested by the parametric bootstrap test with 1,000,000 bootstrap replicates.

3.6. Vibratome sectioning

Untransformed Dionaea leaves were embedded in 5% (w/v) agar (Nacalai Tesque) in water and cut into 100-μm sections by vibratome VT1200 (Leica). Images of sections are taken using microscope BX51 (Olympus) equipped with a DS-Fi1c color camera (Nikon).

3.7. Approximation of decay curve of $[Ca^{2+}]_{cyt}$

Using nls function in R (Milliken et al., 1990), I estimated the $[Ca^{2+}]_{cyt}$ decay curves using two-phase exponential equation (1), one-phase exponential equation (2) and linear equation (3) by non-linear and linear least squares regression.

$$g(t) = ae^{bt} + ce^{dt} + e \quad (1)$$

$$g(t) = ae^{bt} + c \quad (2)$$

$$g(t) = at + b \quad (3)$$

where $g(t)$ is $[Ca^{2+}]_{cyt}$, t is time, a to e are parameters.

3.8. Glands observation

Lobes were cut by razor blade and mounted to the 35mm dish (Falcon) by double sided tape and immersed for 0.5 h to a buffer containing 0.1 mM KCl (Wako), 10 mM $CaCl_2$

(Wako), 20 mM sorbitol (Wako), and 5 mM 2-[Nmorpholino] ethanesulfonic acid (Dojindo Laboratories) adjusted with 2-Amino-2-hydroxymethyl-1,3-propanediol (Wako) to pH 6(Escalante-Perez et al., 2011). Most distal sensory hairs were mechanically stimulated by needles. Stereoscopic images and videos were taken using a SZX16 (Olympus) as same as method of "Microscopy".

3.9. La^{3+} addition treatment

Leaves were cut by scissors at the proximal end of the petioles, and wait for 3 minutes to avoid the effect of the wounding stimulus, then observed the response to mechanical stimulus as samples before treatment. Wait until calcium level went back to the basal level for 3 minutes and leaves were placed in the 35mm dish (Falcon) and added 8 ml of ultrapure water with 0.1 % (v/v) Silwet-L77 (BMS) or 20 mM $LaCl_3$ (Wako) with 0.1 % (v/v) Silwet-L77 (BMS). Silwet-L77 (BMS) was added to avoid the accidental leaf closure due to the surface tension during the immersion in the solution. After 30 minutes immersion, Supernatant was removed and wait for 3 minutes, then observed the response to mechanical stimulus as samples after treatment. Stereoscopic images and videos were taken using a SZX16 (Olympus) as same as method of "Microscopy".

3.10. Scanning electron microscopy

Samples were immediately frozen by liquid nitrogen after harvesting, and observed using TM3030Plus (HITACHI), TM4000Plus (HITACHI), or XL 30 (PHILIPS) microscopes.

3.11. RNA extraction and library preparation

Developmental stages cannot be observed and characterized without dissection, because the adaxial-abaxial margin was curled inward. I thus measured the length of the leaf blades and stages, and defined the leaf blades curled inward at 0 – 550 μm in size as stage 2, those at 550 – 750 μm in size as stage 3, and more than 750 μm in size as stage 4, where the thresholds of the length of the leaf blades were determined by minimizing the number of samples which is misclassified to the wrong stage (minimization of the false positive rates). Shoot apices with leaf primordia were defined as stage 1 and leaves which leaf blades were opened were defined as stage 5. Leaves at each stage were collected into different 2 mL microcentrifuge tubes with a φ5 mm zirconia bead in three biological replicates. Tubes were immediately frozen by liquid nitrogen and stored. Frozen tissues were homogenized using TissueLyser (Qiagen) for 2 min at 30 Hz, and resuspended in PureLink™ Plant RNA Reagent (Thermo Scientific) and total RNA were directly extracted using Direct-zol RNA MiniPrep Plus kit (Zymo Research). Total RNA quality and quantity were determined using 2100 Bioanalyzer (Agilent) and NanoDrop (Thermo Scientific). Libraries for RNA-sequencing were prepared from total RNA using TruSeq Stranded mRNA HT Sample Prep Kit (Illumina) based on the manufacturer's instruction. Sequencing was performed on HiSeq1500 (Illumina) instrument at the conditions of 200 base pairs paired-end reads.

4. Results

4.1. Establishment of the transformation method in Dionaea

To observe spatiotemporal cytosolic [Ca^{2+}] changes in Dionaea, I tested to transform excised leaves with agrobacterium carrying a construct for constitutive expression of sGFP (Chiu et al., 1996; Maekawa et al., 2008; Mano et al., 2014) (pSB111U2-sGFP, Fig. 2a). Based on the number of leaves expressing sGFP, etiolated leaves had a significantly higher transformation rate (97% [*n* = 96]) than non-etiolated leaves (46% [*n* = 91]) (two-tail *p*-value= 4.8e-12 by Fisher's exact test). Furthermore, shoot regeneration rates from etiolated leaves were significantly higher under continuous dark conditions (55% [*n* = 60]) than under continuous light conditions (27% [*n* = 60]) (two-tail *p*-value = 0.0028 by Fisher's exact test). From 77 excised etiolated leaves, I obtained seven transgenic plants that constitutively and ubiquitously expressed sGFP (Fig. 3). During infection, agrobacterium should pass through the cell wall to enter the cytoplasm. There is a possibility that etiolated leaves have cell wall properties that is more suitable for infection by agrobacteria than green leaves.

Using the same procedures, I next produced plants transformed with a construct for constitutive expression of the calcium sensor protein GCaMP6f, which contains a cpEGFP fluorescent moiety (Chen et al., 2013; Maekawa et al., 2008) (pSB111U2-GCaMP6f, Fig. 2b). Five transgenic plants were obtained from 245 excised etiolated leaves. When non-excised leaves of GCaMP6f transgenic Dionaea were placed on ice, cpEGFP fluorescence increased in both leaf lobes and petioles (Fig. 1c), as reported for cold-treated leaves of *Arabidopsis thaliana* (Knight and Knight, 2000). Cytosolic localization of cpEGFP fluorescence was observed in a cut leaf blade (Fig. 4).

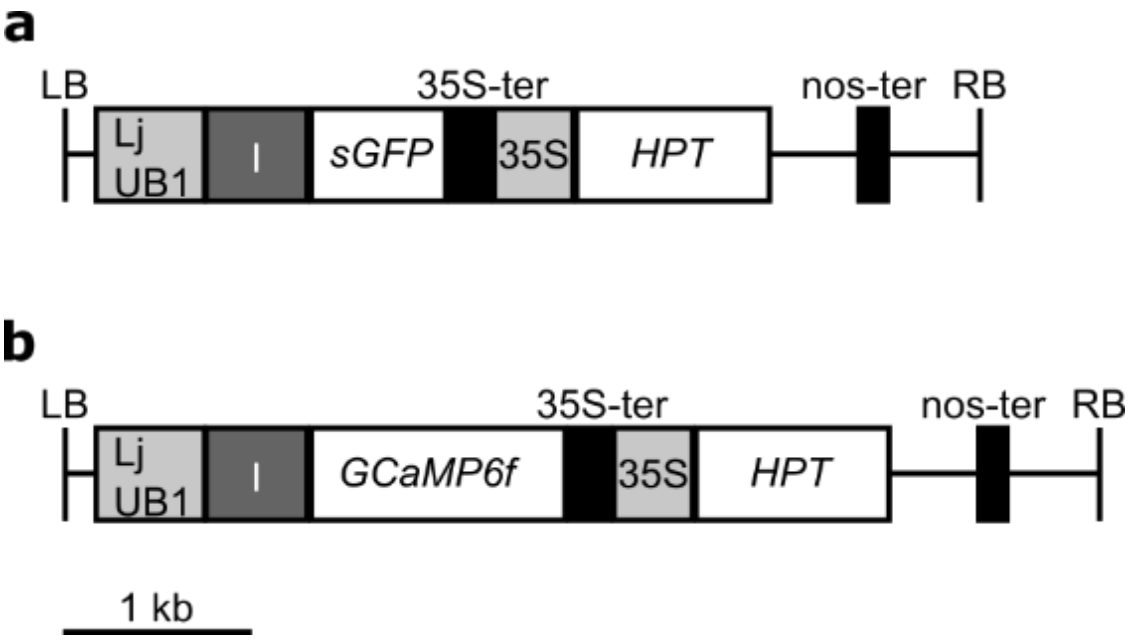

Fig. 2: Construction of the sGFP (a) and GCaMP6f (b) vectors.

a, **b**, Shematic representations of the T-DNA regions of the pSB11U2-sGFP(Maekawa et al., 2008; Chiu et al., 1996) (**a**) and pSB11U2-GCaMP6f (Chen et al., 2013; Maekawa et al., 2008) (**b**) binary vectors. LB, left border; LjUB1, *Lotus japonicus POLYUBIQUITIN* promoter(Maekawa et al., 2008); I, first intron of the *L. japonicus POLYUBIQUITIN* gene(Maekawa et al., 2008); *sGFP*, *sGFP* gene(Chiu et al., 1996); *GCaMP6f*, *GCaMP6f* gene(Chen et al., 2013); 35S-ter, CaMV 35S terminator(Odell et al., 1985); 35S, CaMV 35S promoter(Odell et al., 1985); *HPT*, *HYGROMYCIN PHOSPHOTRANSFERASE* gene(Waldron et al., 1985); nos-ter, the terminator of the nopaline synthase gene(Depicker et al., 1982); and RB, right border.

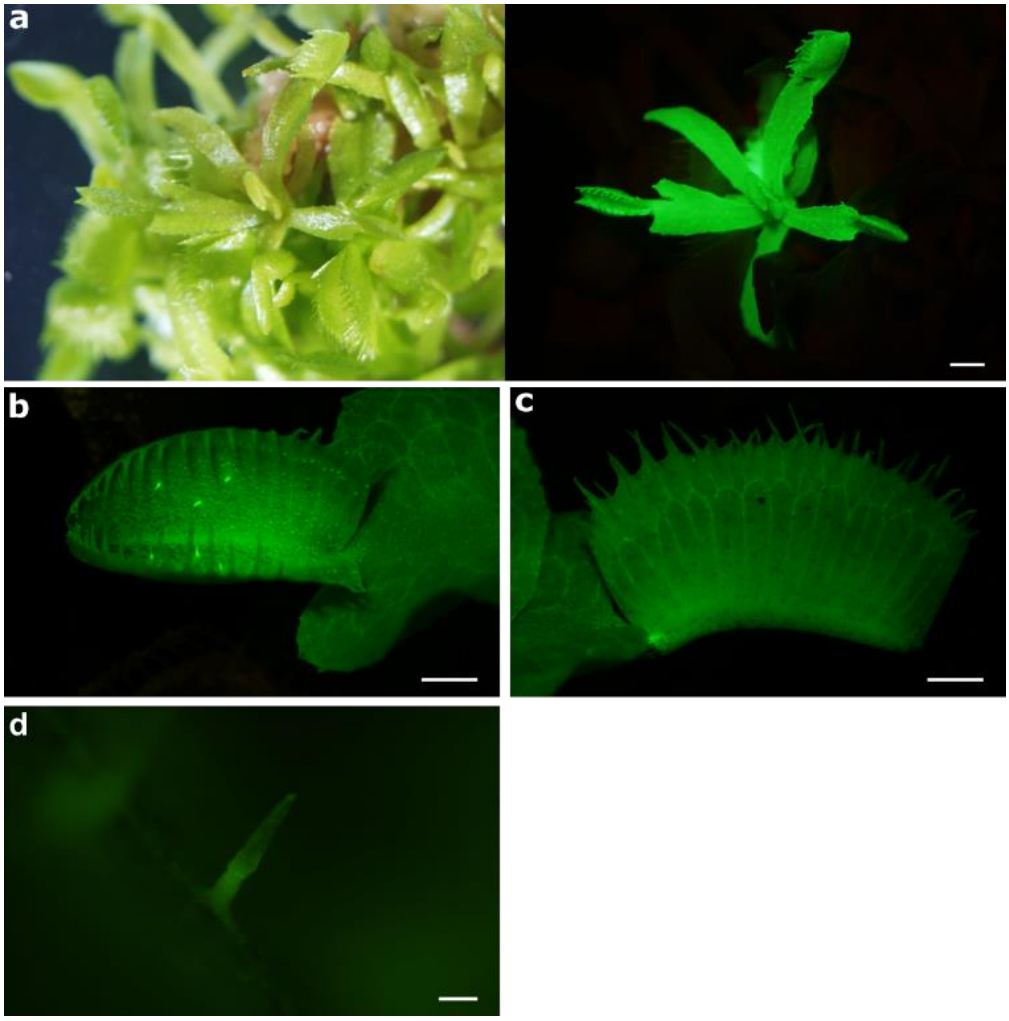

Fig. 3: Transgenic Dionaea constitutively expressing sGFP.

a, Bright-field image (left) and fluorescence image (right) of regenerated plants from an excised etiolated leaf 130 days after infection. A single regenerated plant shows sGFP signal.

b, **c**, Fluorescence images (adaxial **[b]** and abaxial **[c]**) of a transgenic Dionaea plant constitutively expressing sGFP.

d, Fluorescence image of a sensory hair of a transgenic Dionaea plant constitutively expressing sGFP.

Scale bars, 1 mm in (**a**), (**b**), and (**c**); 100 μm in (**d**).

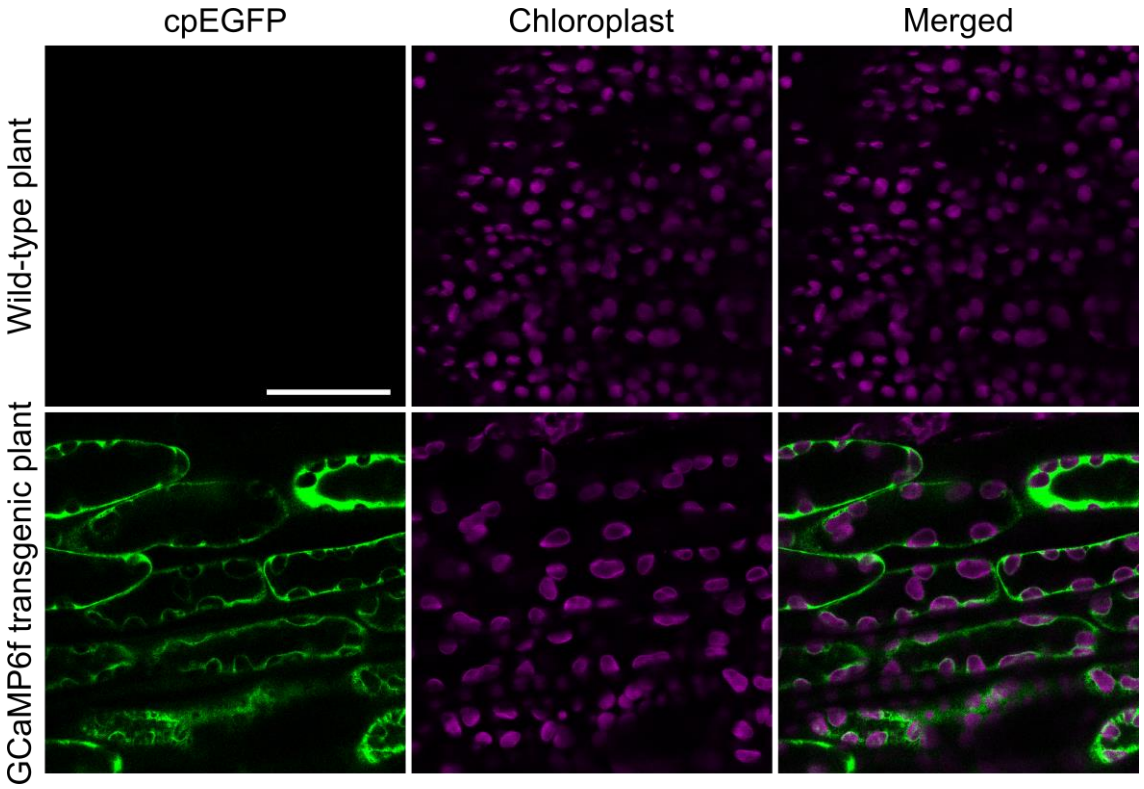

Fig. 4: Cytosolic localization of GCaMP6f protein.

A cpEGFP fluorescence image of GCaMP6f (left), an auto fluorescence image of chloroplasts (middle), and a merged image (right) were taken with confocal microscopy in the razor-blade cut face of a leaf blade at the central area (Fig. 5h). GCaMP6f signals are induced by the cut wounding. Scale bar, 100 μm.

4.2. Response to the first mechanical stimulus in GCaMP6f transgenic Dionaea

I mechanically stimulated the distal part of a sensory hair of GCaMP6f Dionaea by tilting until a change in angle was observed under the microscope using a needle, and then released the needle from the sensory hair within 1 second, then observed that cpEGFP fluorescence increased within 0.02 s at the base of the hair (Fig. 5a), where the sensory cells that generate action potentials are located (Benolken and Jacobson, 1970). Over time, fluorescence intensity continued to increase in the sensory hair (Fig. 5a), and fluorescence spread radially from the sensory hair to the surrounding leaf tissue and fluorescence changes were also observed in small sessile glands and some of the digestive glands which are not pigmentated (Fig. 5c, d, Fig. 6, Video 1 and Video 2). There are both possibilities that the observed fluorescence changes of the glands were derived from the glands themselves or derived from the leaf blade cells and transmitted the glands which are not pigmentated. Fluorescence also propagated from one lobe of the leaf to the other (Fig. 5e, f left, Fig. 7 and Video 3). In the abaxial view, fluorescence was not detected in the midrib (Fig. 5f right). This suggests that fluorescence is propagated in the epidermis and/or parenchyma adaxial to the midrib, but not in the midrib and tissue surrounding the midrib, both of which are connected to the petiole (Fig. 5f and g). This is consistent with the observation that fluorescence did not propagate into the petiole (Fig. 5f).

I could not localize fluorescence to specific cells because of the difficulty of observing intact cells deep within the leaf and the need to avoid wound-induced fluorescence that would be caused by physical dissection (Fig. 4). The fluorescence signal extended laterally as far as the area where secondary leaf veins, which run perpendicularly from a primary vein in the midrib toward the leaf edges, begin to

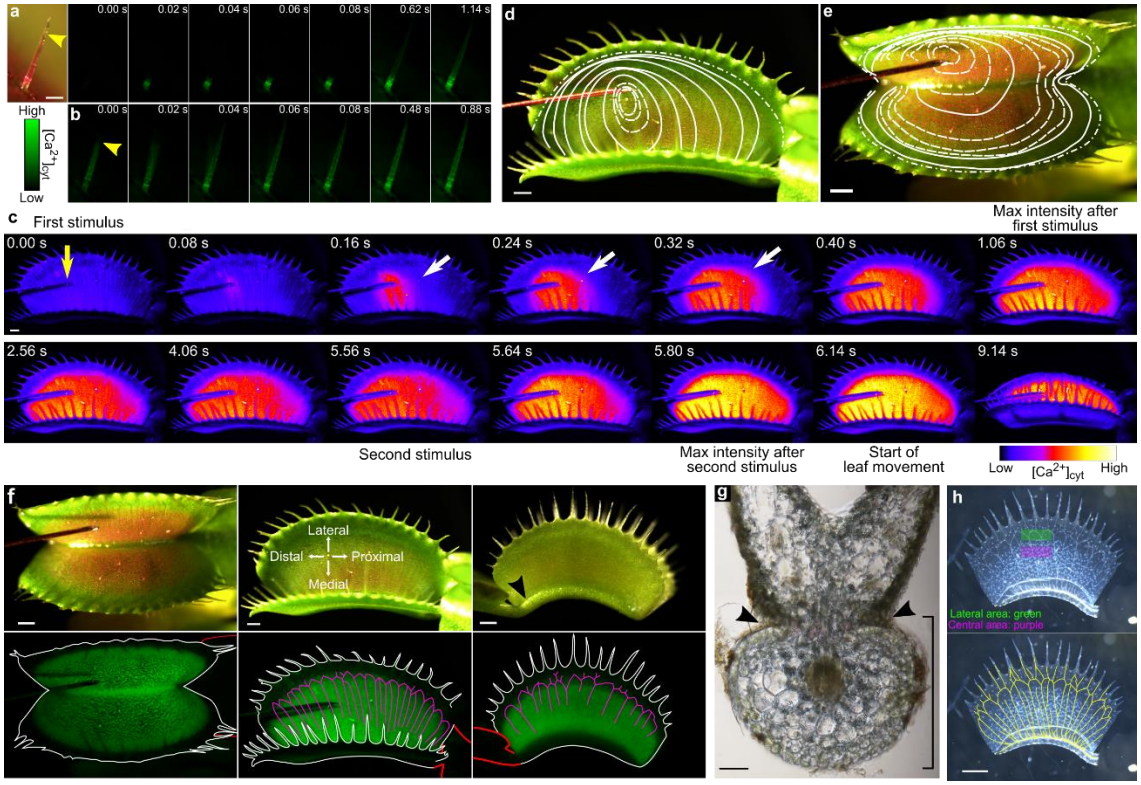

Fig. 5: A $[Ca^{2+}]_{cyt}$ increase propagates from the sensory hair to the leaf blade after mechanical stimulation.

a–b, Bright-field (**a**, leftmost) and fluorescence (others) images of a sensory hair stimulated by a needle at the indicated position by arrow-heads. Seconds (s) from the first (**a**) or second (**b**) stimulus is indicated. Rightmost fluorescence images are the frames with the maximum intensity scored after the stimulus. Maximum intensity was measured across the whole pictured area. The second stimulus was applied 13.08 s after the first stimulus.

c, Fluorescence images of a GCaMP6f Dionaea leaf blade after a sensory hair was stimulated with a needle (yellow arrow). Frames were extracted in pseudocolor from those shown in Video 1. Seconds (s) after the first stimulus are indicated. White arrows indicate sensory hairs with fluorescence despite not having been mechanical stimulated. The leaf closed after the second stimulus. Max intensity was measured across the whole pictured area.

d–e, Propagation of the $[Ca^{2+}]_{cyt}$ increase following the first mechanical stimulation to a sensory hair, indicated on bright-field images of the leaf shown in **c** (**d**) and in Fig. 7 (**e**). Boundaries of the propagated area are shown every 0.02 s (white dashed line) and 0.08 s (white solid line). The boundary of the maximum propagated area is shown by a white dash-dotted line, 1.06 s (**d**) and 0.60 s (**e**) after application of the mechanical stimulus,

respectively.
f, Bright-field (top) and fluorescence (bottom) images of the adaxial (left and middle) and abaxial (right) sides of leaves showing the frame at which the maximum intensity after the mechanical stimulation was scored. Intensity was measured across the whole pictured area. White and red lines indicate outlines of a leaf blade and petiole, respectively. Magenta lines indicate leaf veins around the lateral boundary of fluorescence.
g, Transverse section of tissue around the midrib. Black arrowheads indicate borders between fluorescent and non-fluorescent regions in the abaxial surface. The midrib is indicated by a bracket.
h, Bright-field images of a cleared leaf blade. Lateral and Central areas used in the logistic regression analysis are indicated in green and magenta in the upper image. Secondary veins are indicated in the lower image (yellow lines).
Scale bars, 200 μm in (**a**) and (**b**); 1 mm in (**c**)-(**f**) and (**h**); 100 μm in (**g**).

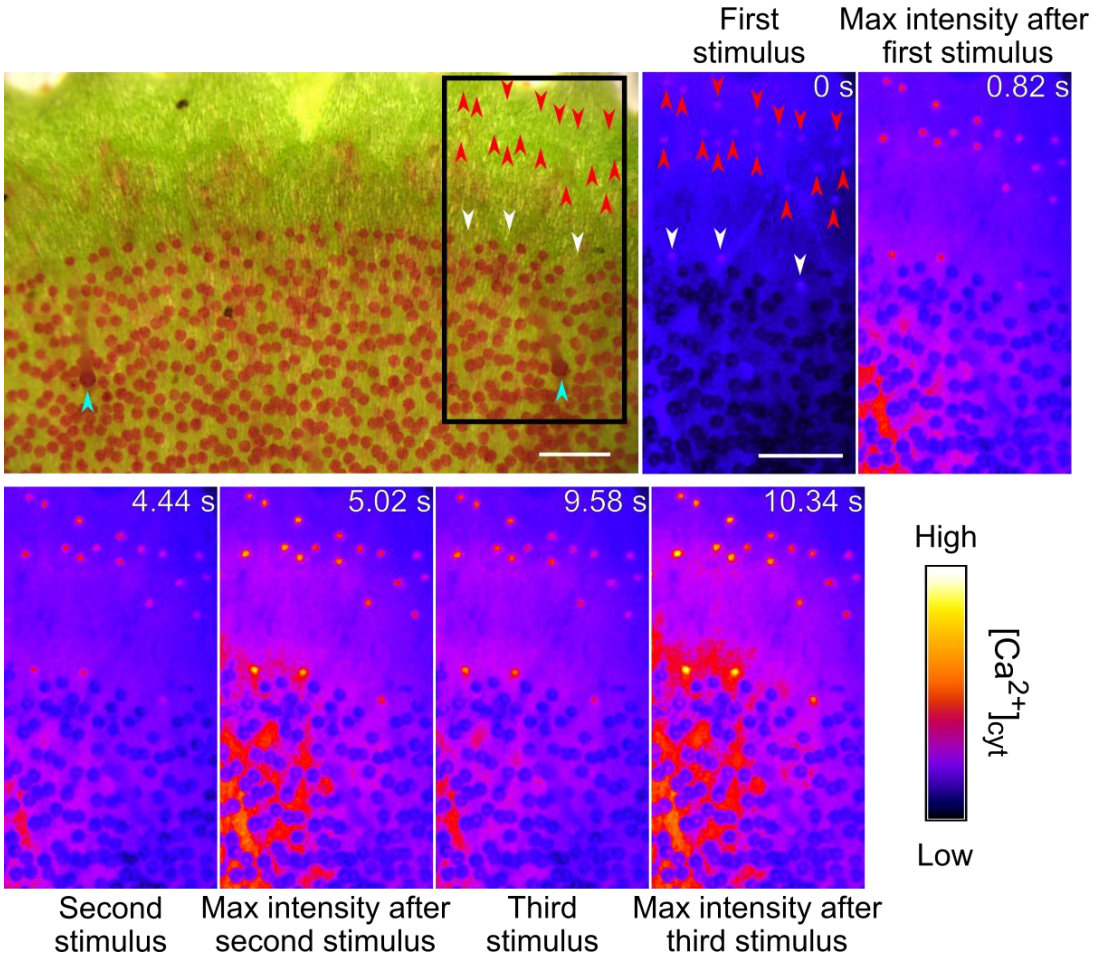

Fig. 6: GCaMP6f signals in the lateral side of digestive glands and small sessile glands by a series of mechanical stimuli.

A bright field image (upper leftmost) and fluorescence images (others) at the leaf blade. A pictured area of the fluorescence images corresponds to the square area in the bright field image. Sensory hairs are indicated by light blue arrow-heads. The most distal sensory hair (left light blue arrow-head) was stimulated by a needle. Pseudocolor images were extracted from those shown in Video 2. Seconds (s) after the first stimulus are indicated. Some of the digestive glands at the lateral side increased fluorescence intensities by each mechanical stimulus (white arrow-heads), as same as small sessile glands (red arrow-heads). All of these glands were invisible in the bright field image because of those green colors (white and red arrow-heads in the bright field image). We could not detect the increase of GCaMP6f signals in most of the digestive glands by any of the three stimuli, although a previous study(Escalante-Perez et al., 2011) with FURA-2 calcium indicator showed that the increase of FURA-2 signal was not detected by the first and second mechanical stimuli but was by the third stimulus. Scale bar, 1 mm.

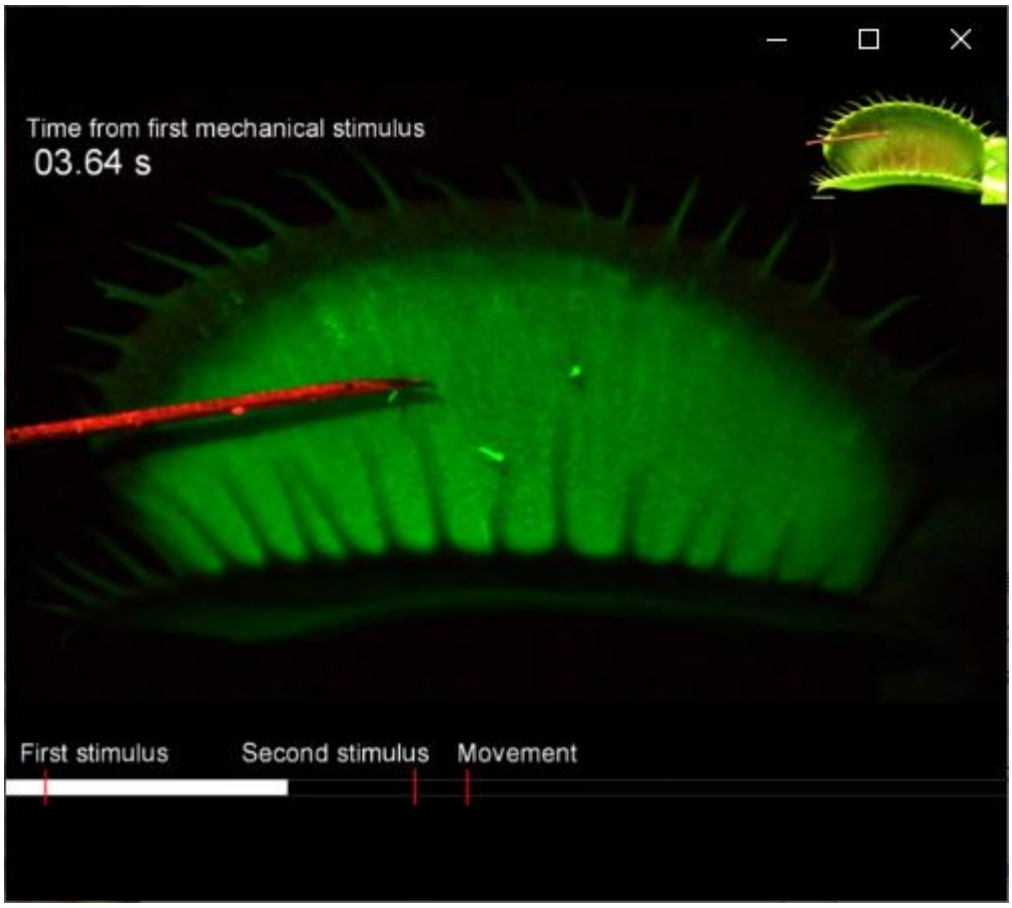

Video 1 | The $[Ca^{2+}]_{cyt}$ increases following mechanical stimulation of a sensory hair of the GCaMP6f-transgenic Dionaea.

The video is played at real time speed. Time (seconds, s) after the first mechanical stimulus is indicated. Scale bar, 2 mm.
(https://drive.google.com/file/d/1r_dcmht76XVm420Sb7CpdoKTz3tCEYl-/view)

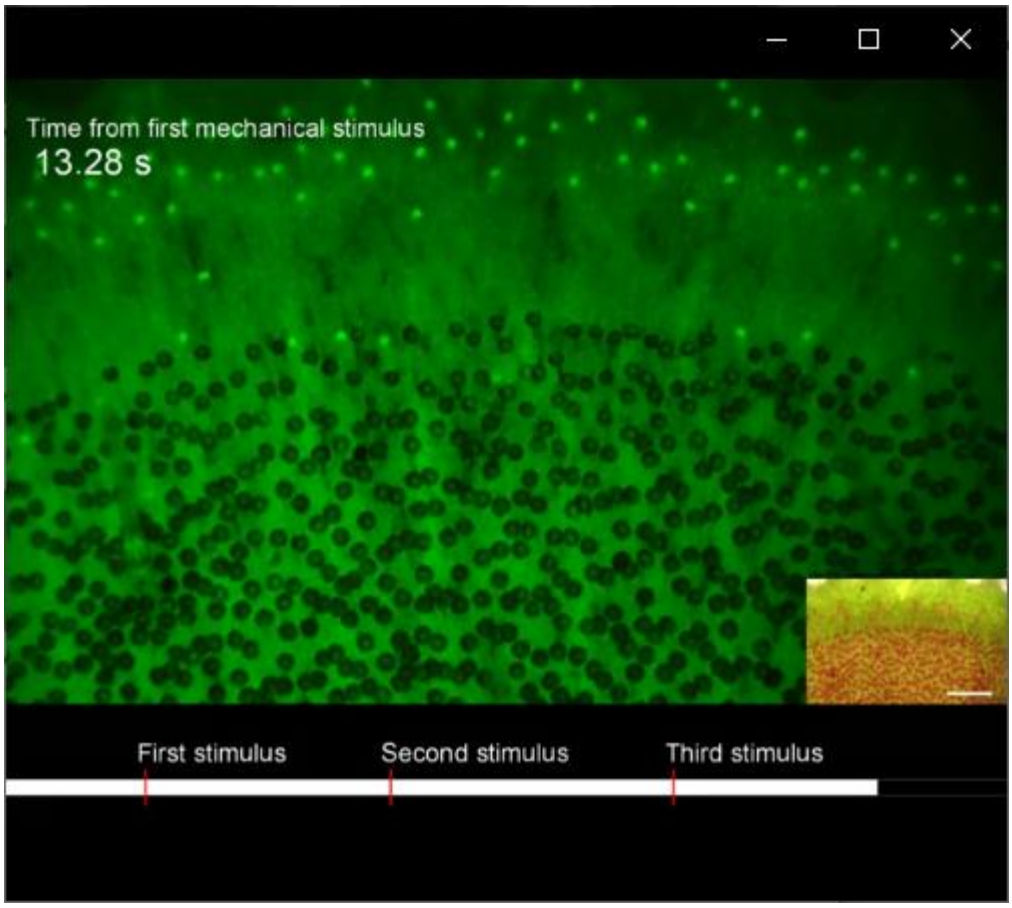

Video 2 | $[Ca^{2+}]_{cyt}$ increase at some of lateral digestive glands and small sessile glands following mechanical stimulation of a sensory hair of the GCaMP6f-transgenic Dionaea.

The video is played by real time speed. Time (seconds, s) after the first mechanical stimulus is indicated. Scale bar, 1 mm.
(https://drive.google.com/file/d/1r_dcmht76XVm420Sb7CpdoKTz3tCEYl-/view)

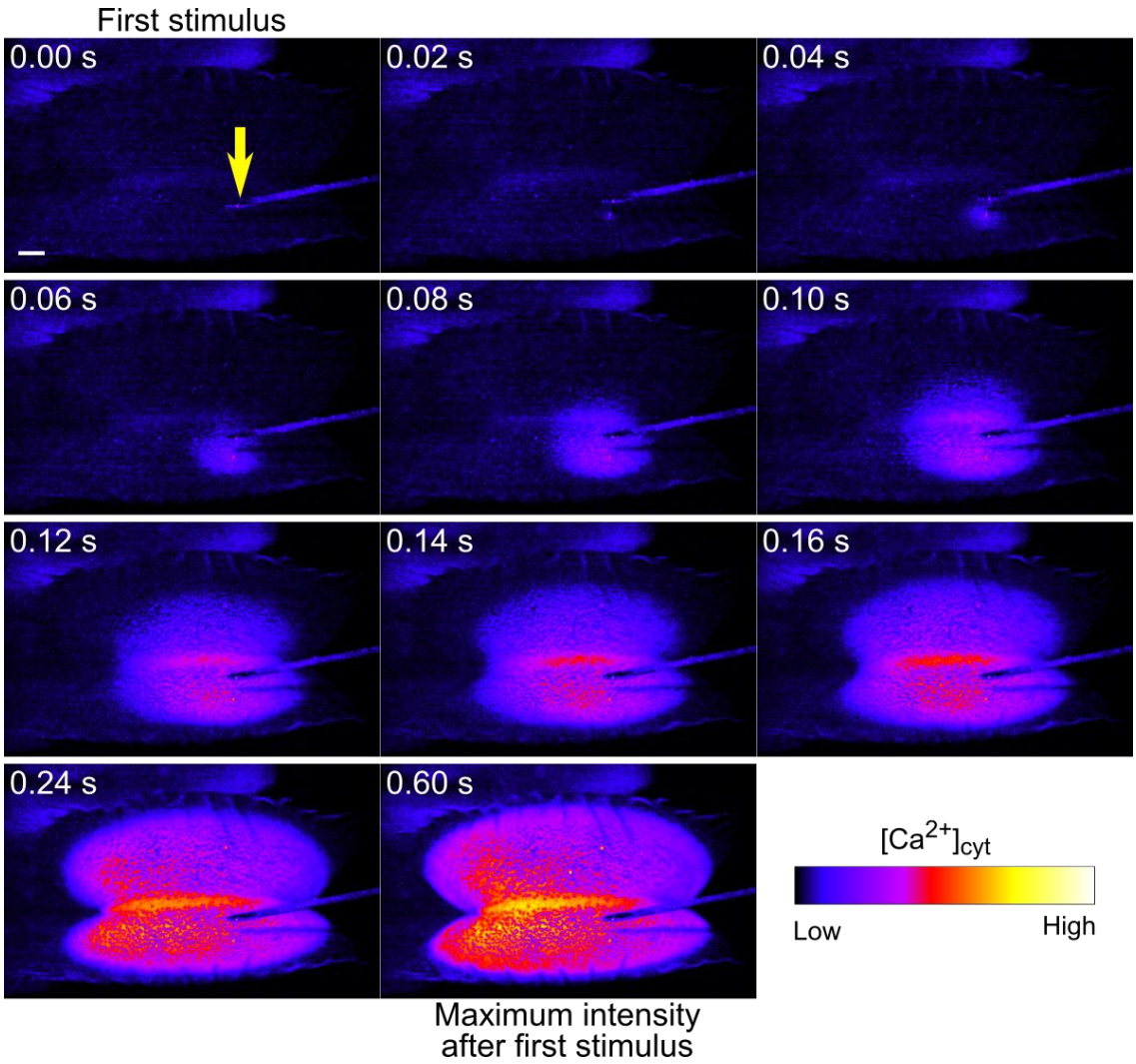

Fig. 7: The $[Ca^{2+}]_{cyt}$ increase induced by a mechanical stimulation propagates from the one lobe of a blade to the other.

Fluorescence images of a GCaMP6f Dionaea leaf, after a sensory hair was subjected to the first mechanical stimulus with a needle (yellow arrow). Frames are extracted in pseudocolor from those shown in Video 3. Seconds (s) after the first stimulus is indicated. Maximum intensity was measured at the whole pictured area. Scale bar, 1 mm.

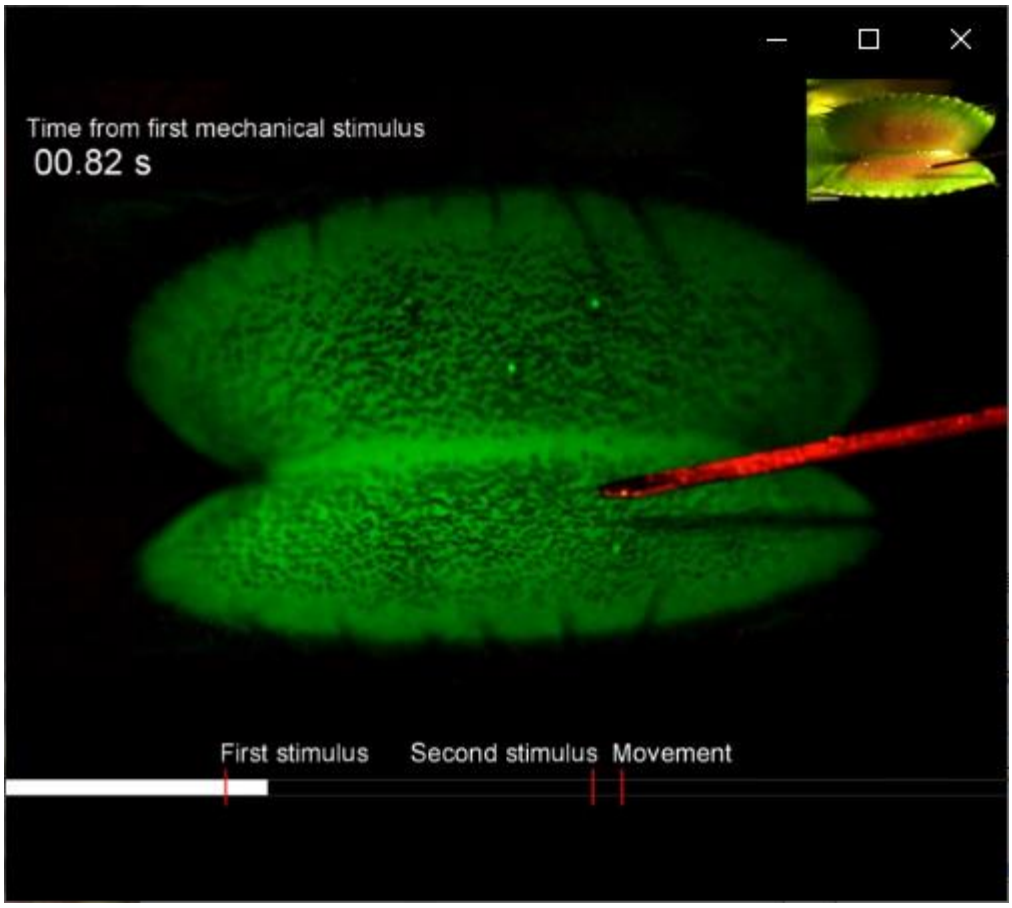

Video 3 | The $[Ca^{2+}]_{cyt}$ increase propagates from one lobe of a blade to the other in GCaMP6f-transgenic Dionaea.

The video is played at real time speed. Time (seconds, s) after the first mechanical stimulus is indicated. Scale bar, 2 mm.
(https://drive.google.com/file/d/1r_dcmht76XVm420Sb7CpdoKTz3tCEYl-/view)

branch and merge with neighboring veins (Fig. 5h). This was the furthest lateral spread observed on both the adaxial and abaxial sides of the leaf (Fig. 5f).

4.3. Propagation velocity of the Ca^{2+} wave

The average propagation velocity in the medial direction (53 ± 8.2 mm/s [mean ± s.e.m., *n* = 8 leaves]) was faster than that in the lateral direction (20 ± 6.8 mm/s [mean ± s.e.m., *n* = 8 leaves]). Average velocities in the proximal and distal directions were similar to that in the lateral direction (23 ± 3.2 mm/s [mean ± s.e.m., *n* = 8 leaves] and 21 ± 3.2 mm/s [mean ± s.e.m., *n* = 8 leaves], respectively) (Fig. 5d and Fig. 8a). The velocity did not change when the fluorescence crossed a leaf vein or the midrib (Video 3). The Ca^{2+} wave velocities resulting from stimulation of a sensory hair and those caused by wounding to the leaf blade were not distinguished (Fig. 8c, Fig. 9, Table 1 and Video 4). It should be noted that the same action potentials are produced in response to mechanical stimulation and wounding (Pavlovič et al., 2017).

Fluorescence of unstimulated sensory hairs increased when the wave front reached them (Fig. 5c and Video 1). This is consistent with the observation that leaf closure can be induced with a second stimulus to any sensory hair, not only the one that received the first stimulus. It is noteworthy that the Ca^{2+} wave velocities resulting from stimulation of a sensory hair as well as those caused by wounding to the leaf blade are approximately 50 to 20 times faster than those caused by wounding to petioles in *A. thaliana* (1.089 mm/s)(Toyota et al., 2018) and in Dionaea (1.2 ± 0.17 mm/s [mean ± s.e.m., *n* = 5 leaves]) (Fig. 8d, Fig. 10 and Video 5).

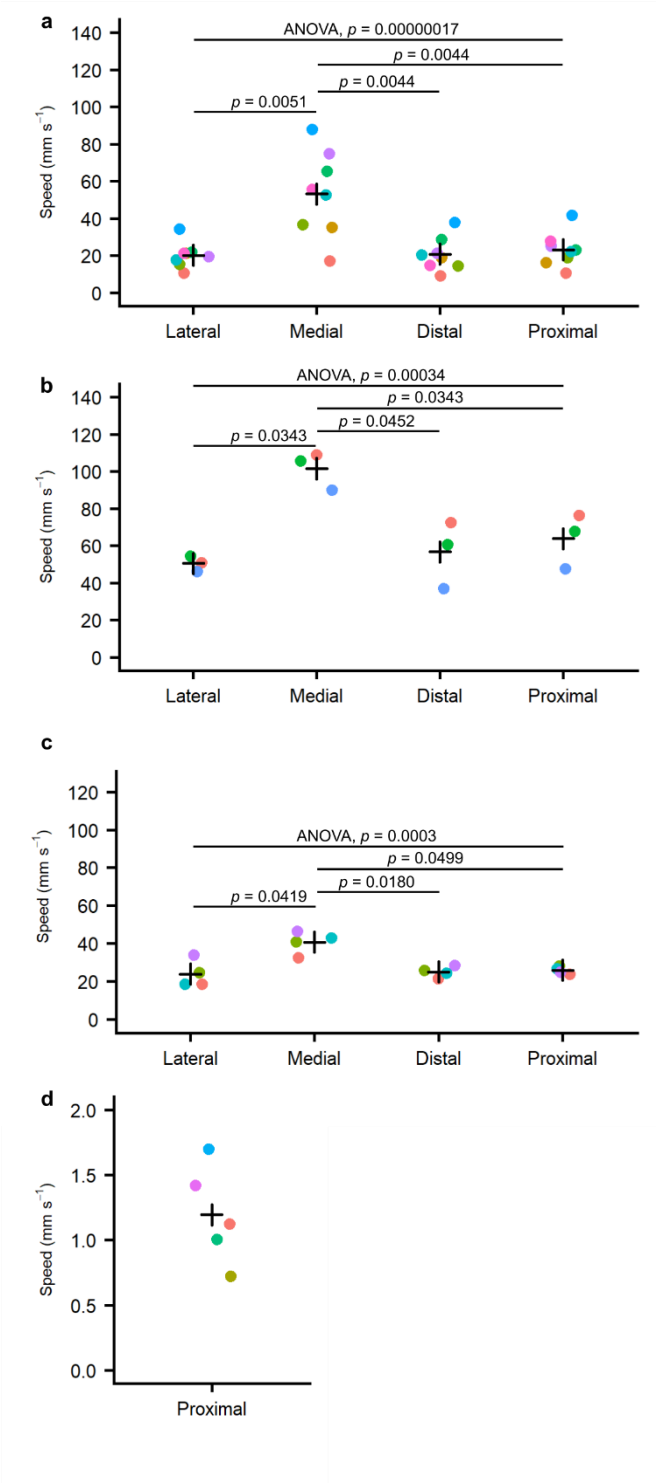

Fig. 8: Propagation velocity of the $[Ca^{2+}]_{cyt}$ increase.

a–c, Propagation velocity of the $[Ca^{2+}]_{cyt}$ increase from a stimulated sensory hair (**a** and **b**) or from a wounded tissue (**c**). Fluorescence were measured after the first stimulus (**a**) (n = 8), second stimulus (**b**) (n = 3), and wounding stimulus by needle at the central area (**c**) (n = 4) were applied. The most distal sensory hairs were mechanically stimulated

after 5.18, 5.52 and 5.54 s from the first stimuli. Mean values are indicated by reticles. Velocities were measured in four directions from the stimulated site (Fig. 1b and Fig. 5f top middle). Two-way analysis of variance without replication with Holm's sequentially rejective Bonferroni procedure was used to calculate two tail *p*-values.
d, Propagation velocity of $[Ca^{2+}]_{cyt}$ increase by wounding (n = 5). The midrib was cut at the proximal end of the leaf blade by scissors. The cut position corresponds to that in the previous study in *A. thaliana*(Toyota et al., 2018). Mean values are indicated by reticles. Velocities were measured in the proximal direction from the stimulated site (Fig. 10).

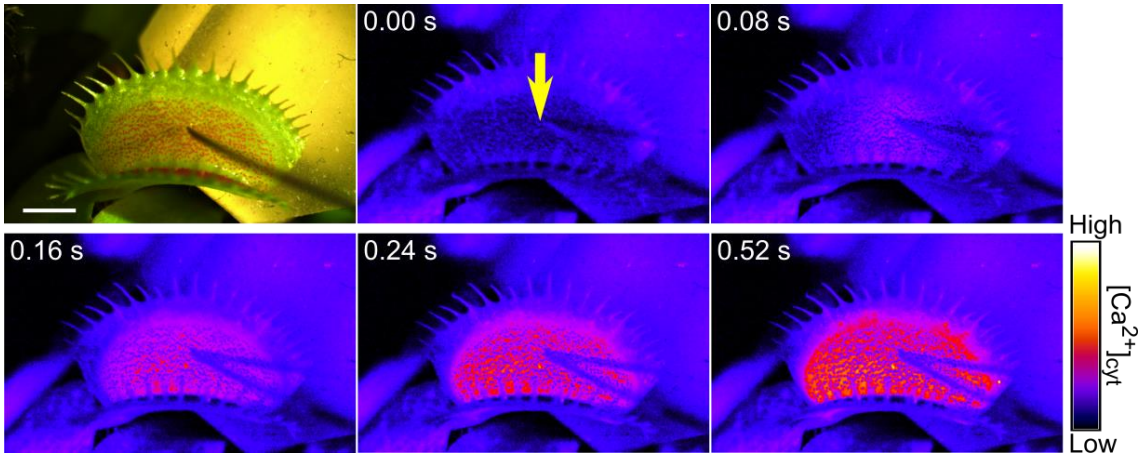

Fig. 9: The $[Ca^{2+}]_{cyt}$ increase induced by a wounding stimulus to the leaf blade. Bright field image (upper leftmost) and fluorescence images (others) of a GcaMP6f Dionaea leaf wounded by a needle (yellow arrow). Frames were extracted with pseudocolor from those shown in Video 4. Seconds (s) after the wounding stimulus is indicated. Scale bar, 2 mm.

Table 1 Summary of the velocities of calcium signal propagation

Measured signal	Stimulus	Velocity			
		Proximal (mm/s)	Distal (mm/s)	Medial (mm/s)	Lateral (mm/s)
Action potential[a]	First stimulus	54–81	63	113–115	-
	Second stimulus	-	-	250	-
Calcium signal[b]	First stimulus	23 ± 3.2 [*n* = 8]	21 ± 3.2 [*n* = 8]	53 ± 8.2 [*n* = 8]	20 ± 2.4 [*n* = 8]
	Second stimulus	64 ± 8.5 [*n* = 3]	57 ± 10[*n* = 3]	102 ± 5.8 [*n* = 3]	51 ± 2.3 [*n* = 3]
	Wounding stimulus to leaf blade	26 ± 0.97 [n = 4]	25 ± 1.4 [n = 4]	41 ± 3.0 [n = 4]	24 ± 3.6 [n = 4]
	Wounding stimulus to petiole	1.2 ± 0.17 [n = 5]	-	-	-

[a]Velocity of the action potential in the leaves of Dionaea following stimulation in previous studies. The action potential triggered by the first stimulus is cited from Fig. 4 of Sibaoka (1966)(Sibaoka, 1966), and by the second stimulus is from Sibaoka (1980)(Sibaoka, 1980).

[b]Velocity of the signal propagated from the stimulated site in each direction. Velocities are shown as mean ± s.e.m. [*n* = number of leaves measured].

Video 4 | The $[Ca^{2+}]_{cyt}$ increases following wounding at the leaf blade of the GCaMP6f-transgenic Dionaea.

The video is played by real time speed. Time (seconds, s) after the wounding stimulus is indicated. Distal and proximal sensory hairs are indicated by white arrows. Scale bar, 2 mm.

(https://drive.google.com/file/d/1r_dcmht76XVm420Sb7CpdoKTz3tCEYl-/view)

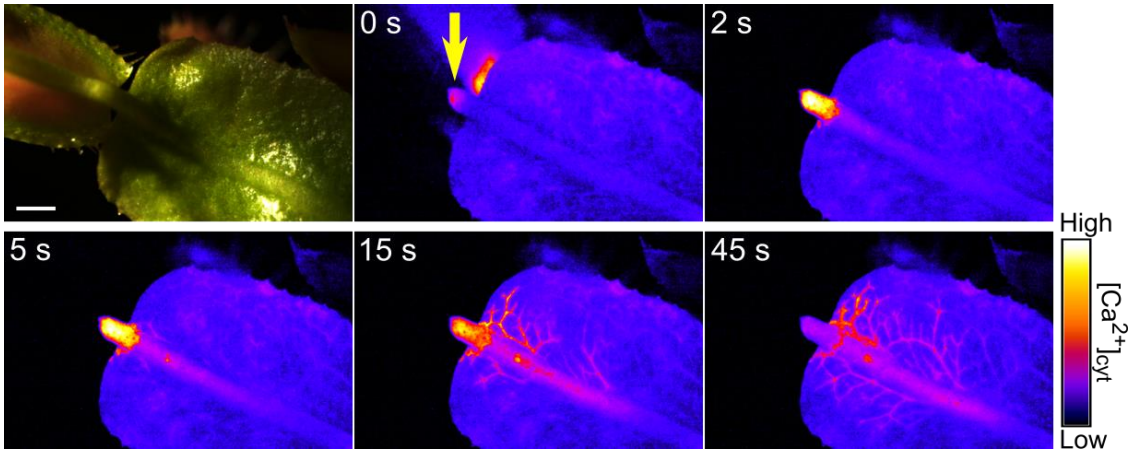

Fig. 10: $[Ca^{2+}]_{cyt}$ increase induced by a wounding stimulus to the midrib propagates along the midrib.

Bright field image (upper leftmost) and fluorescence images (others) of a GCaMP6f Dionaea leaf wounded by cutting with scissors (yellow arrow) the midrib at the proximal end of the leaf blade. Frames were extracted with pseudocolor from those shown in Video 5. Seconds (s) after the wounding stimulus is indicated. Scale bar, 2 mm.

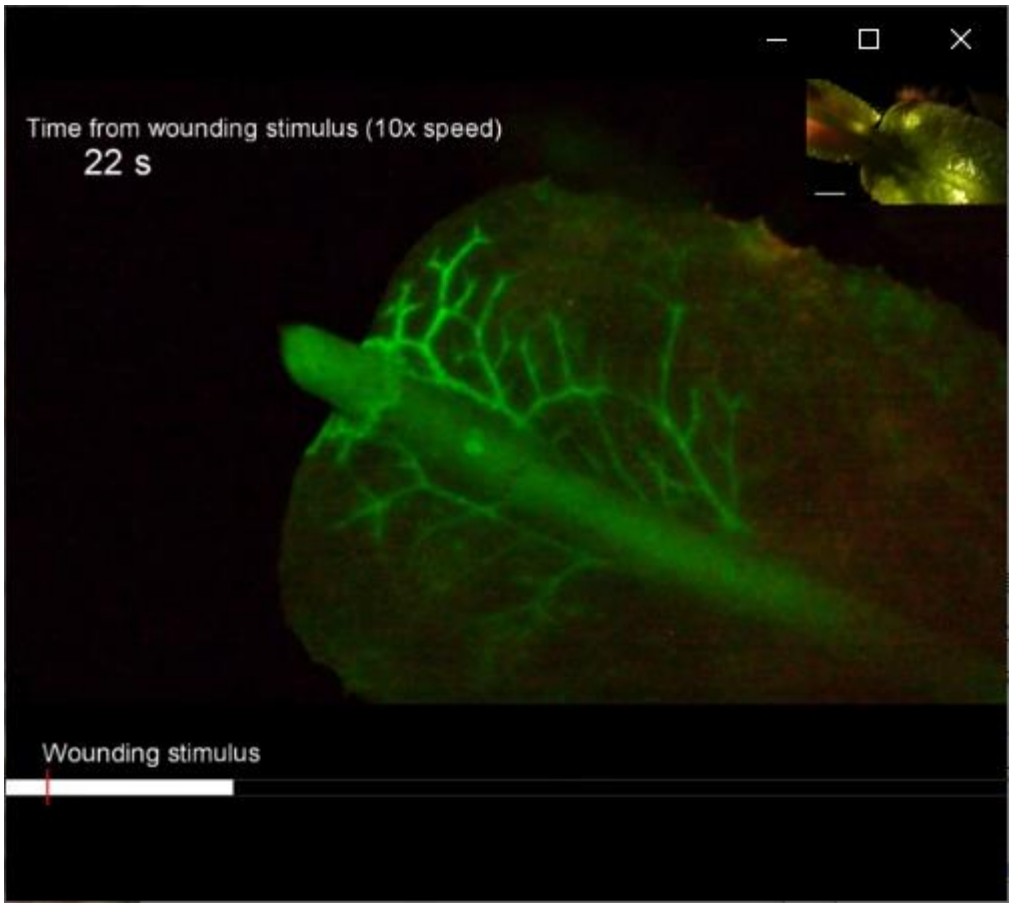

Video 5 | The $[Ca^{2+}]_{cyt}$ increases following wounding at the midrib of the boundary between the leaf blade and petiole of the GCaMP6f-transgenic Dionaea.
The video is played at 10 times the speed. Time (seconds, s) after wounding is indicated. Scale bar, 2 mm.
(https://drive.google.com/file/d/1r_dcmht76XVm420Sb7CpdoKTz3tCEYl-/view)

4.4. Response to the second mechanical stimulus in GCaMP6f transgenic Dionaea

I next observed Ca^{2+} dynamics following a second stimulus. The second stimulus further increased the signal intensity of the stimulated sensory hair (Fig. 5b), then propagated radially to mostly the same area as the first stimulus did, and the leaf closed (Fig. 5c, Fig. 11 and Video 1). Average propagation velocities for the second stimulus were approximately two to three times faster than those for the first stimulus in all four directions (Fig. 5c, Fig. 8b, Table 1 and Video 1), suggesting that cells with an increased $[Ca^{2+}]_{cyt}$ caused by the first stimulus are more sensitive to a second stimulus. The leaf area with increased fluorescence was indistinguishable from the area that changed tissue curvature and strain during the leaf closure in a previous study (Forterre et al., 2005; Sachse et al., 2020).

These results and the Ca^{2+} requirement of the snap movement (Hodick and Sievers, 1988, 1989; Fagerberg and Allain, 1991) are concordant with the previous proposal that $[Ca^{2+}]_{cyt}$ increases during excitation and is involved in triggering movement (Hodick and Sievers, 1988). However, to clarify the causality between $[Ca^{2+}]_{cyt}$ and movement, future genetic studies are necessary. The anisotropic differences in propagation velocities of the $[Ca^{2+}]_{cyt}$ increase and the acceleration of propagation velocities in response to the second stimulus (Fig. 8 and Table 1) are qualitatively in agreement with the behavior of leaf action potentials (Sibaoka, 1966). However, the action potentials propagate at 60 to 170 mm/s after the first stimulus and 250 mm/s after the second stimulus (Sibaoka, 1966, 1980), much faster than the propagation of $[Ca^{2+}]_{cyt}$ changes (20 to 53 mm/s after the first stimulus, 51 to 102 mm/s after the second stimulus; Table 1). Furthermore, lateral movement of the $[Ca^{2+}]_{cyt}$ wave stops once it has reached the area where the secondary veins branch (Fig. 5f), while

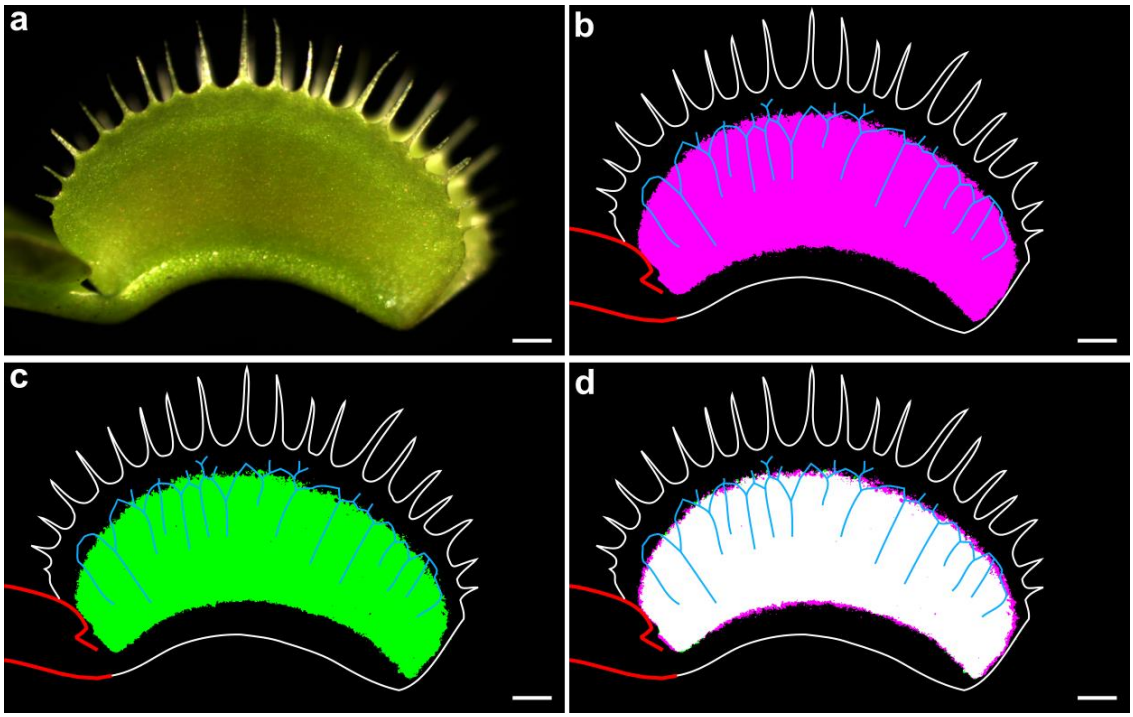

Fig. 11: Leaf areas exhibiting a $[Ca^{2+}]_{cyt}$ increase following the first and second stimulation overlapped.

Bright-field image (**a**) and the cpEGFP fluorescence changed area at the maximum intensity frame after application of the first (**b**) and second (**c**) stimulus. Merged image of (**b**) and (**c**) is shown in (**d**). Maximum intensity was measured across the whole pictured area. White and red lines mark the boundary of the leaf blade and petiole, respectively. Blue lines indicate leaf veins around the lateral boundary of fluorescence. The second stimulus was applied 12.06 s after the first stimulus. Scale bar, 1 mm.

action potentials continue beyond that boundary to reach the margin of the leaf blade (Sibaoka, 1966). Since different experimental setups result in variable velocities of action potentials (Volkov, 2019), a measurement of action potentials in GCaMP6f Dionaea together with [Ca2+]cyt changes is necessary to further investigate the relationship between [Ca2+]cyt wave and action potential.

4.5. Logistic regression analysis of the fluorescence intensity change

To investigate whether the need for two stimuli can be explained by there being a $[Ca^{2+}]_{cyt}$ threshold for movement (Hodick and Sievers, 1988), I quantitated GCaMP6f after a mechanical stimulus to a sensory hair (Fig. 12a and b). I hypothesized that thresholds of $[Ca^{2+}]_{cyt}$ to trigger the movements are different between leaves and leaves sense relative differences between the $[Ca^{2+}]_{cyt}$ after the first stimulus and the second stimulus. Based on this hypothesis, I normalized fluorescence intensity in the lateral and central areas of leaf blades (Fig. 5h) every 0.02 s fluorescence intensity at time "t" to the maximum intensity after the first stimulus, to yield relative intensity "F_t" (Fig. 12a and Fig. 13). The first stimulus triggered an elevation in fluorescence intensity, which then gradually decreased in both areas of the leaf (Fig. 12a and b). Fluorescence increased additively in response to the second stimulus in both areas, and then the leaf closed. The maximum fluorescence intensity after the second stimulus was higher than that reached after the first stimulus. Fluorescence intensities after the start of leaf movement could not be accurately measured because of the rapid movement.

Because movement is triggered by the second stimulus, I measured the residual F_t immediately before the second stimulus (F_{res}), and the maximum F_t just after the second stimulus (F_{max}) (Fig. 12a). Logistic regression analysis showed that F_{res} in both

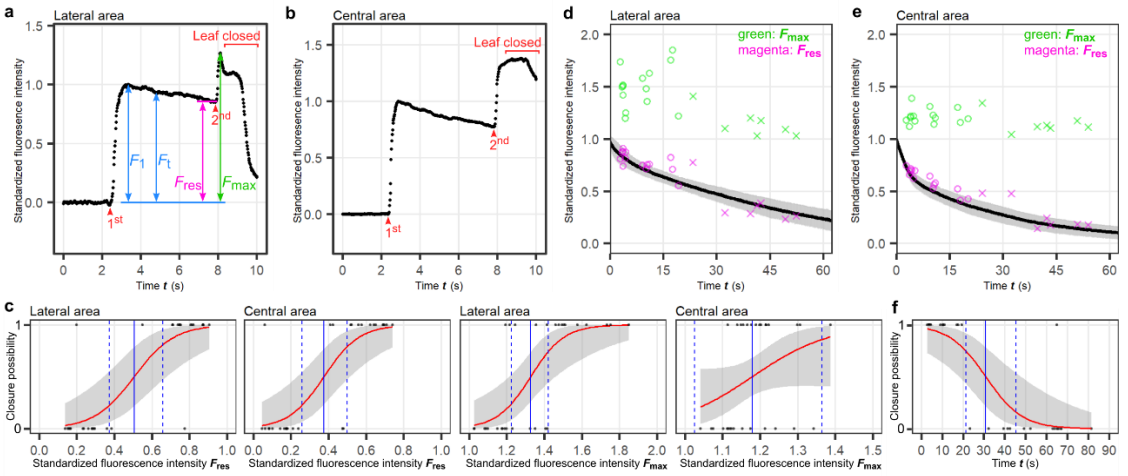

Fig. 12: Quantitative analysis of temporal fluorescence changes after mechanical stimulation and the putative $[Ca^{2+}]_{cyt}$ threshold at which movement is triggered.

a–b, Representative time courses of the normalized fluorescence intensity at time t [F_t] in the lateral (**a**) and central (**b**) areas. First and second stimuli are indicated as "1st" and "2nd", respectively. The leaf closed after the second stimulus. F_1, maximum F_t after the first stimulus before the second stimulus; F_{res}, F_t immediately before the second stimulus; F_{max}, maximum F_t after the second stimulus. Plots of fluorescence intensity without normalization are shown in Fig. 13.

c, Regression curves in the logistic regression analyses of F_{res} at lateral areas (leftmost), F_{res} at central areas (second left), F_{max} at lateral areas (second right), and F_{max} at central areas (rightmost). Leaf states (black dots; 1, closed; 0, open), regression curve (red lines), 95% CI (Confidence Intervals) of the regression curve (gray regions), predicted putative thresholds of F_t to trigger closure of 50% leaves (solid blue lines), and 95% CI of the putative threshold (dashed blue lines) are shown.

d–e, Decay curves of the fluorescence intensity (F_t) after F_1 is reached in the lateral (**d**) and central (**e**) area. The mean (black line) and standard deviation of the mean (grey region) are plotted every 0.02 s (n = 6). F_{res} (magenta) and F_{max} (green) in (**c**) are plotted. Leaves were closed (circles) or not (x).

f, Regression curves in the logistic regression analyses of duration between the first and second stimuli. Leaf states (black dots; 1: close, 0: open), regression curve (red lines), 95% CI of the regression curve (gray regions), predicted putative thresholds of F_t to trigger closure of 50% leaves (solid blue lines), and 95% CI of the putative threshold (dashed blue lines) are shown.

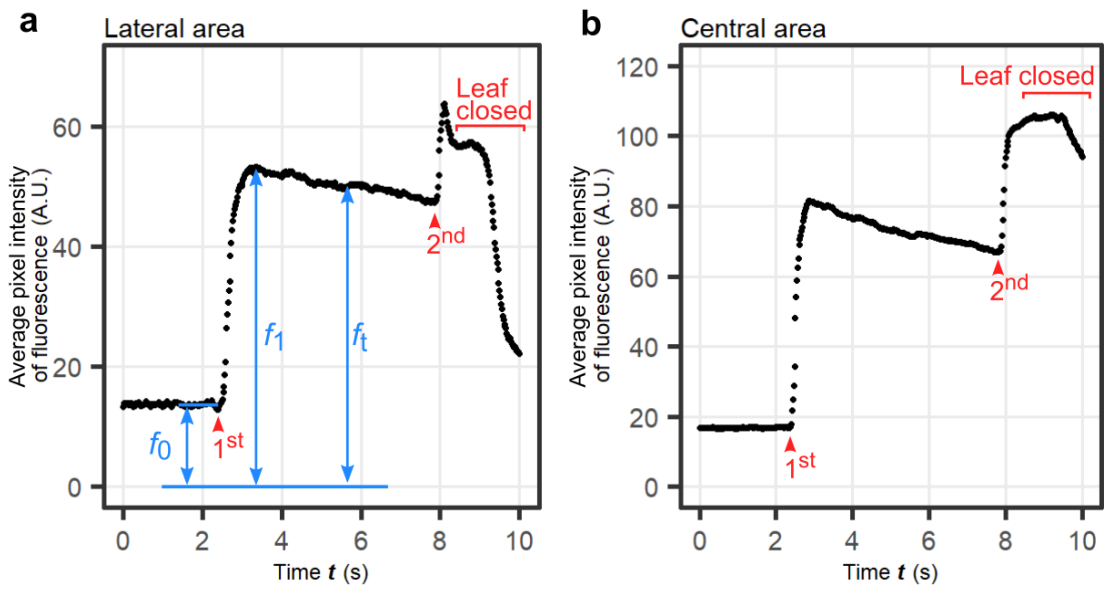

Fig. 13: Procedure for the normalization of fluorescence intensity.

a–b, Representative time courses of the average pixel intensities of fluorescence in the lateral (**a**) and central (**b**) areas without normalization. First and second stimuli are indicated as "1st" and "2nd", respectively. After the second stimulus, the leaf closed. The normalized fluorescence intensity F_t was calculated as $(f_t–f_0) / (f_1–f_0)$, where f_t, averaged pixel intensity of fluorescence at a given time "t"; f_0, averaged f_t of 50 frames 1 s before the first stimulus; f_1, maximum f_t after the first stimulus before the second stimulus.

lateral and central areas were significantly correlated with leaf closure (Fig. 12c and Table 2). However, F_{max} in the lateral area, but not in the central area, were significantly correlated with leaf closure. It is possible that $[Ca^{2+}]_{cyt}$ exceeded the detection range of GCaMP6f in the central area after the second stimulus, because fluorescence intensity was higher in the central area than in the lateral area (Fig. 13). The predicted 95% confidence intervals (CI) of putative threshold F_{res}, where leaf closure is triggered with 50% probability, were 0.3738-0.6598 and 0.2599–0.4999 in the lateral and central areas, respectively (Table 2). The 95% CI of putative threshold F_{max} was 1.226–1.422 in the lateral area. A likelihood ratio test rejected the assumption that leaf closure does not depend on $[Ca^{2+}]_{cyt}$ (Table 2). These results indicate that there are putative $[Ca^{2+}]_{cyt}$ thresholds for immediately before and after the second stimulus that should be met for movement to occur. Since the predicted 95% CI of putative threshold F_{max} (1.226–1.422) is higher than that for F_1 (1.000), a single stimulus cannot raise $[Ca^{2+}]_{cyt}$ over the putative threshold F_{max} and a second stimulus is necessary to meet the putative threshold for movement, at least in the lateral area.

4.6. The decay of Ca^{2+} signal

Next, I examined whether a second stimulus could raise $[Ca^{2+}]_{cyt}$ to the threshold after the memory limit time of 30 s after the first stimulus (Brown and Sharp, 1910; Juniper et al., 1989a). I measured F_t every 0.02 s after the time of F_1 in the absence of a second stimulus (Fig. 12d and e). $[Ca^{2+}]_{cyt}$ decreased with time in both lateral and central areas of the leaf, and decay curves were well fit into the two-phase exponential curves with lower Akaike's Information Criterion compared to other simpler models (Fig. 14). F_{res} and F_{max} in the separate experiments with the second stimulus were plotted on the same

Table 2 Putative thresholds of $[Ca^{2+}]_{cyt}$ and duration with logistic regression analyses

Explanatory variable	Area	Threshold (95% CI)[a]	Odds ratio (95% CI)[b]	Maximum likelihood	Likelihood ratio test[c]
F_{res}	lateral	0.5058 (0.3738–0.6598)	1.165×10^4 (1.32×10^2-1.145×10^7)	$2.2*10^{-4}$	0.000002***
	central	0.3756 (0.2599–0.4999)	4.114×10^4 (2.141×10^2-1.382×10^8)	$9.023*10^{-5}$	0.000008***
F_{max}	lateral	1.327 (1.226–1.422)	7.627×10^4 (1.558×10^2-7.536×10^8)	$8.301*10^{-6}$	0.000044***
	central	1.179 (1.026–1.364)	1.608×10^4 (0.932-3.825×10^9)	$6.17*10^{-9}$	0.063311
Duration	-	30.88 s (21.4–45.42)	0.8917 (0.8093–0.9446)	$3.229*10^{-4}$	0.000001***

[a]Value of F_{max} or F_{res} where half number of the trap leaves close.

[b]Effect size calculated from the regression coefficient.

[a,b]95% CI: predicted 95% confidence intervals of putative threshold.

[c]*** $p < 0.001$ ($n = 30$).

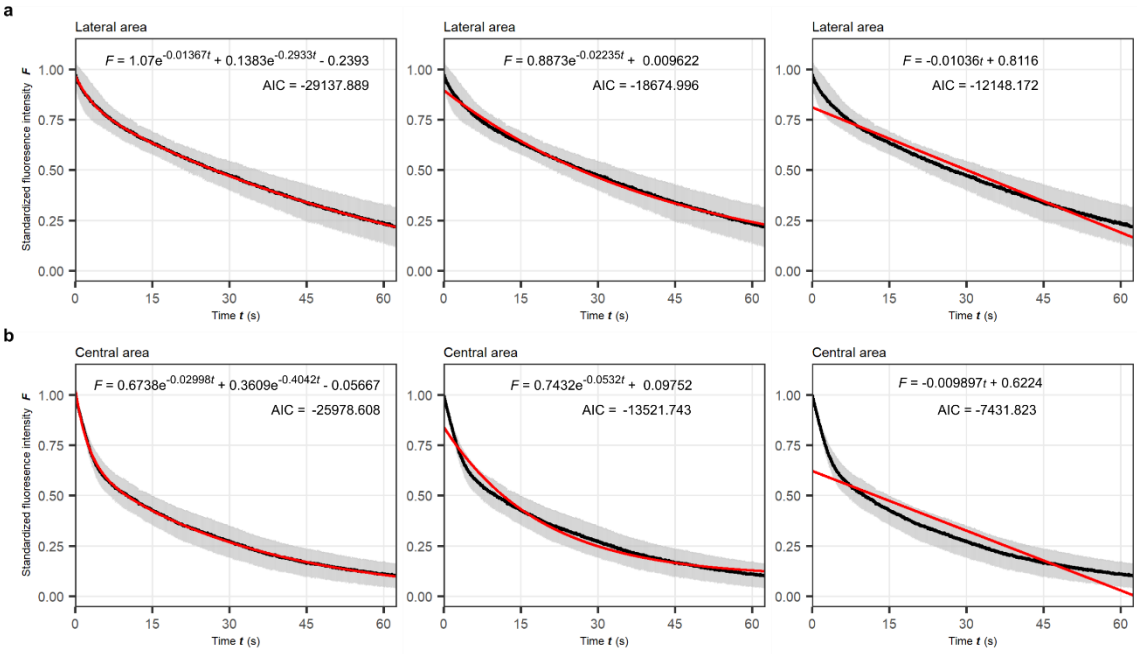

Fig. 14: Fitting of decay curves of fluorescence intensities.

Fitting of decay curves of the fluorescence intensity (F_t) after F_1 in Fig. 12d (lateral area, **a**) and Fig. 12e (central area, **b**) was investigated with linear and non-linear least squares regression. Fitting curves (red lines) were calculated by two-phase exponential decay model (left), one phase exponential decay model (middle), and linear model (right). The mean (black line) and standard deviation of the mean (grey region) are plotted every 0.02 seconds (n = 6). Fitting equations and AICs are indicated in each panel.

graph with showing whether the leaf closed or not at given time (Fig. 12d and e). Leaf closure depends on the time elapsed after F_1 is reached. Logistic regression analysis showed that the putative 50% leaf closure threshold for the duration of the F_1 signal was 30.88 s with 95% CI 21.4–45.42 s (Fig. 12f and Table 2), which concurs with previous studies (Brown and Sharp, 1910; Juniper et al., 1989a). The means of $F_{30.88}$ in the lateral and central areas were 0.4631 ± 0.07214 [mean ± s.e.m., n = 6 leaves] (Fig. 12d) and 0.2638 ± 0.07758 [mean ± s.e.m., n = 6 leaves] (Fig. 12e), respectively, which are within the ranges of 95% CIs of putative F_{res} thresholds (Table 2). These results indicate that the time course of $[Ca^{2+}]_{cyt}$ decay correlates with the duration of the signal produced by the first stimulus, and that the 30-second length of memory is explained by the decay of $[Ca^{2+}]_{cyt}$.

4.7. Response to the third mechanical stimulus

I also investigated whether the third stimulus can rise $[Ca^{2+}]_{cyt}$ over the putative threshold F_{max} and trigger movement, when the second stimulus does not trigger movement. After the third stimulus, F_t at the lateral area reached to the 95% CI of the putative threshold and the leaf closed (Fig. 15, Fig. 16 and Video 6). On the other hand, even when F_t at central area reached to the 95% CI of the putative threshold, the leaf did not close (Fig. 15 and Fig. 16). These results are concordant with the result that F_{max} at lateral area significantly correlate to the movement but F_{max} at central area does not (Table 2).

4.8. Threshold analysis under the artificially controlled Ca^{2+} level

To further investigate relationships between the putative $[Ca^{2+}]_{cyt}$ threshold and movement, two experiments were employed. I found that Dionaea leaves close with no

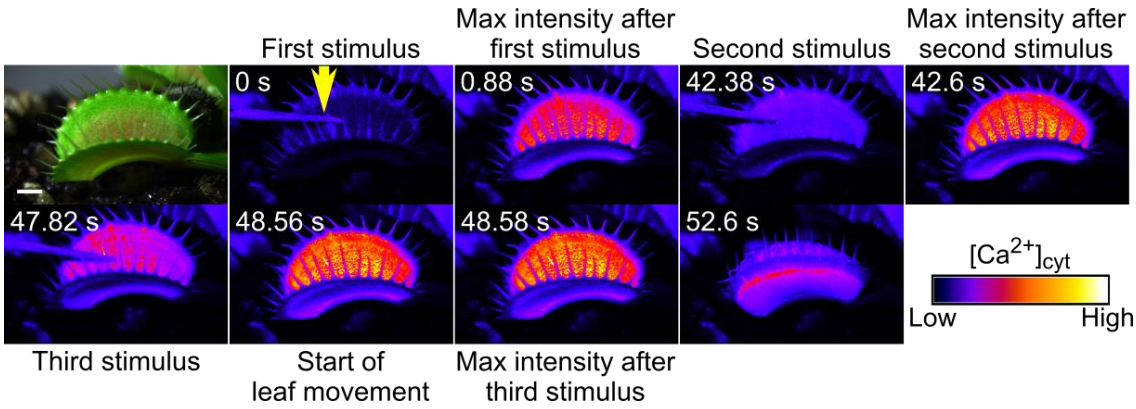

Fig. 15: Bright and fluorescence images of a GCaMP6f Dionaea leaf that closed after the third stimulus.

A bright field image (upper left) and fluorescence images (others) in the adaxial views of a GCaMP6f Dionaea leaf after a sensory hair was stimulated with a needle (yellow arrow). Frames were extracted with pseudocolor from those shown in Video 6. Seconds (s) after the first stimulus are indicated. Leaf moved after the third stimulus. Max intensity was measured across the whole pictured area. Scale bar, 2 mm.

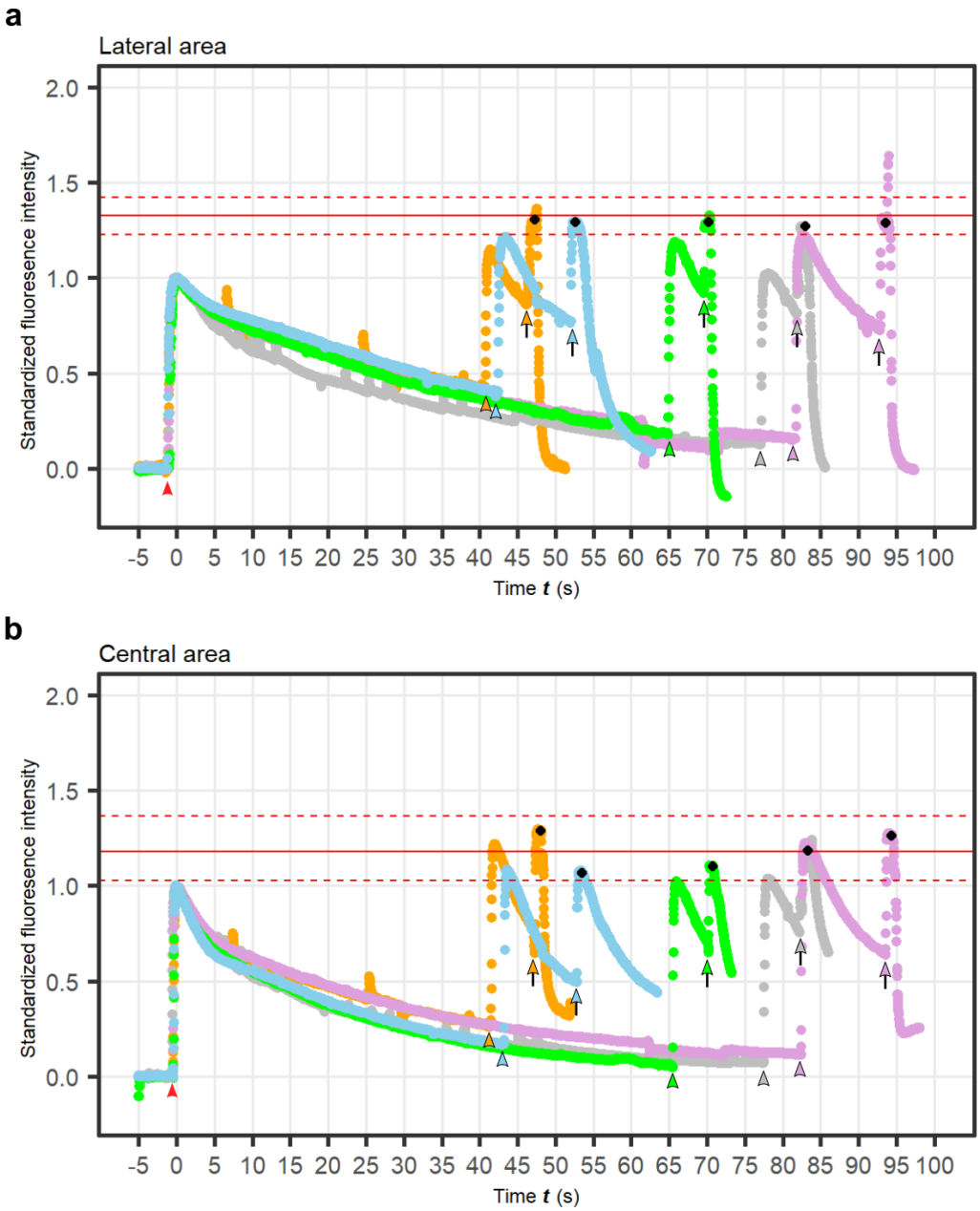

Fig. 16: Temporal fluorescence changes of GCaMP6f Dionaea leaves that did not close by the first and the second mechanical stimuli but closed by the third stimulus. **a–b**, Representative time courses of the normalized fluorescence intensity at time t [F_t] in the lateral (**a**) and the central (**b**) areas (n = 5). Time at the max intensity after the first mechanical stimulus (red arrow-head) is set as 0 second for each experiment. The second and the third stimuli are indicated by arrow-heads and arrows, respectively. The color of arrow-heads in the second and the third stimuli correspond to that of the plots. Time points when leaf movement started are indicated by black dots. Putative thresholds for the movement (red lines) and 95% CIs (red dotted lines) are taken from Table 2.

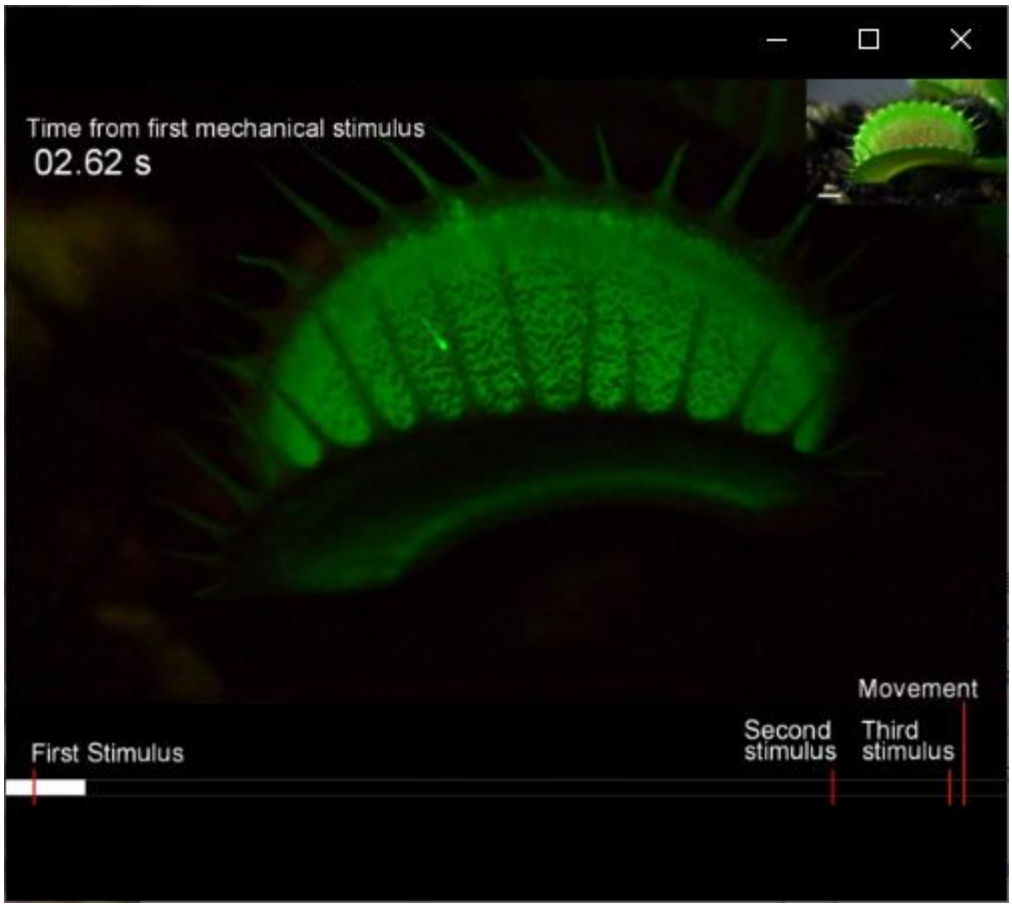

Video 6 | Leaf movement is triggered by third stimulus when leaf do not close by the second stimulus.

The video is played at real time speed. Time (seconds, s) after the first mechanical stimulus is indicated. Scale bar, 2 mm.
(https://drive.google.com/file/d/1r_dcmht76XVm420Sb7CpdoKTz3tCEYl-/view)

mechanical stimuli within one minute, when a leaf is removed from a stem at the attached position and the basal part of a petiole was immediately put in water. Even with no mechanical stimuli, the $[Ca^{2+}]_{cyt}$ signal increased two or three times and the leaf closed (Fig. 17, Fig. 18 and Video 7). Before the leaf closure, $[Ca^{2+}]_{cyt}$ signals reached within the 95% CIs of the putative threshold (Fig. 18). As the second experiment, I immersed a whole leaf in the calcium channel blocker La^{3+} solution (Hodick and Sievers, 1989; Fagerberg and Allain, 1991) to reduce $[Ca^{2+}]_{cyt}$ levels. Although I do not know the reason, after 30 min immersion with no mechanical stimuli, fluorescence intensity increased at the marginal area of the leaf blade, where Ca^{2+} waves caused by a mechanical stimulus to the sensory hair did not reach (Fig. 19). In a whole leaf immersed in water as a control, the second mechanical stimulus raised $[Ca^{2+}]_{cyt}$ over the putative threshold to close the leaf (Fig. 20a, Fig. 21a and Video 8). On the other hand, $LaCl_3$ treated leaves did not move even after the third stimulus and $[Ca^{2+}]_{cyt}$ did not reach the 95%CI of the putative threshold at lateral area (Fig. 20b, Fig. 21b and Video 9). These results are concordant with the hypothesis that leaf movement is triggered when the $[Ca^{2+}]_{cyt}$ surpasses the threshold for the movement.

4.9. Definitions of the developmental stages in Dionaea

To investigate the candidates of calcium signaling related genes in Dionaea, I performed a transcriptome analysis of Dionaea at a series of developmental stages.

Development of the Dionaea leaf was described in previous studies (Kurtz, 1876; De Candolle, 1876; Fraustadt, 1877), however, leaf blade development was observed only by the sections cut by a plane perpendicular to the midrib, and three-dimensional morphology of the leaf blade development and temporal order in which

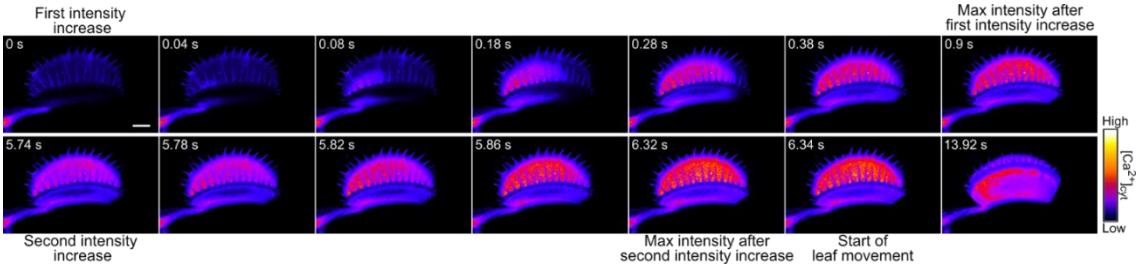

Fig. 17: Fluorescence images of a GCaMP6f Dionaea leaves, whose petiole base was put in water.

Fluorescence images of a GCaMP6f Dionaea leaf after the basal part of petiole were cut by scissors and the cut face was immediately put in water. Frames were extracted with pseudocolor from those shown in Video 7. Seconds (s) after the first intensity increased are indicated. Max intensity was measured across the whole pictured area. Scale bar, 2 mm.

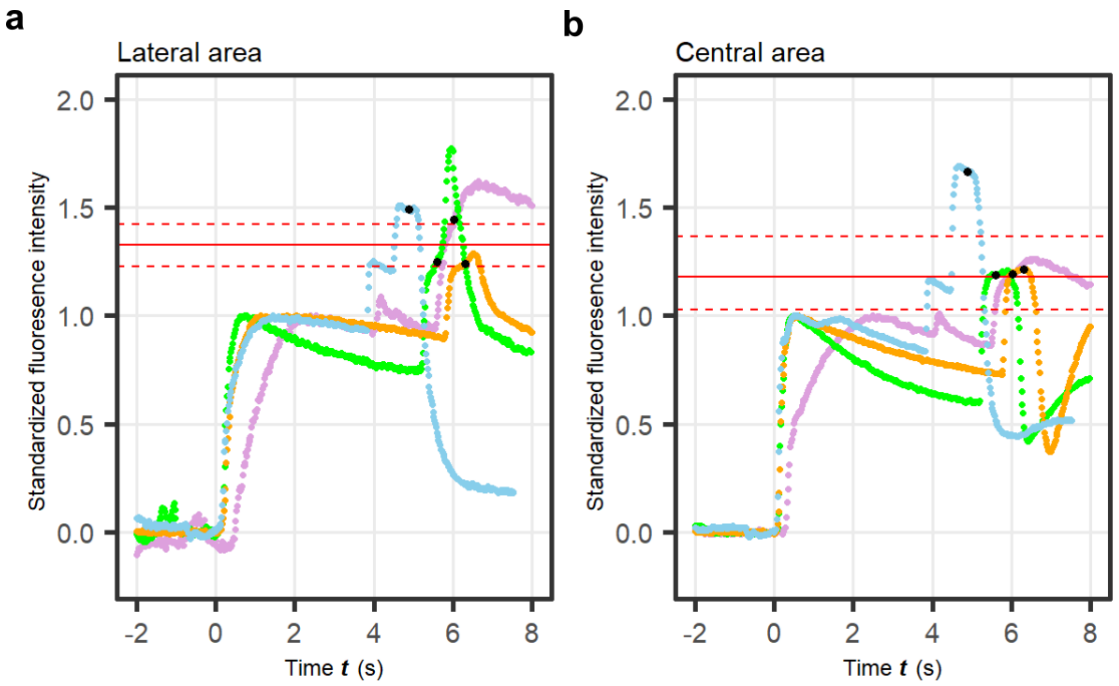

Fig. 18: Temporal fluorescence changes with no mechanical stimuli in a GCaMP6f Dionaea leaf whose petiole base is put in water.

a–b Representative time courses of the normalized fluorescence intensity at time t [F_t] in the lateral (**a**) and central (**b**) areas of a leaf whose petiole base was put in water (n = 4). Time when fluorescence intensity started to increase without a stimulus is indicated as 0 second. Even though leaves were not mechanically stimulated, two or three successive increases of signals were detected. Time points when leaf movement started are indicated by black dots. Putative thresholds for the movement (red lines) and their 95% CIs (red dotted lines) are taken from Table 2.

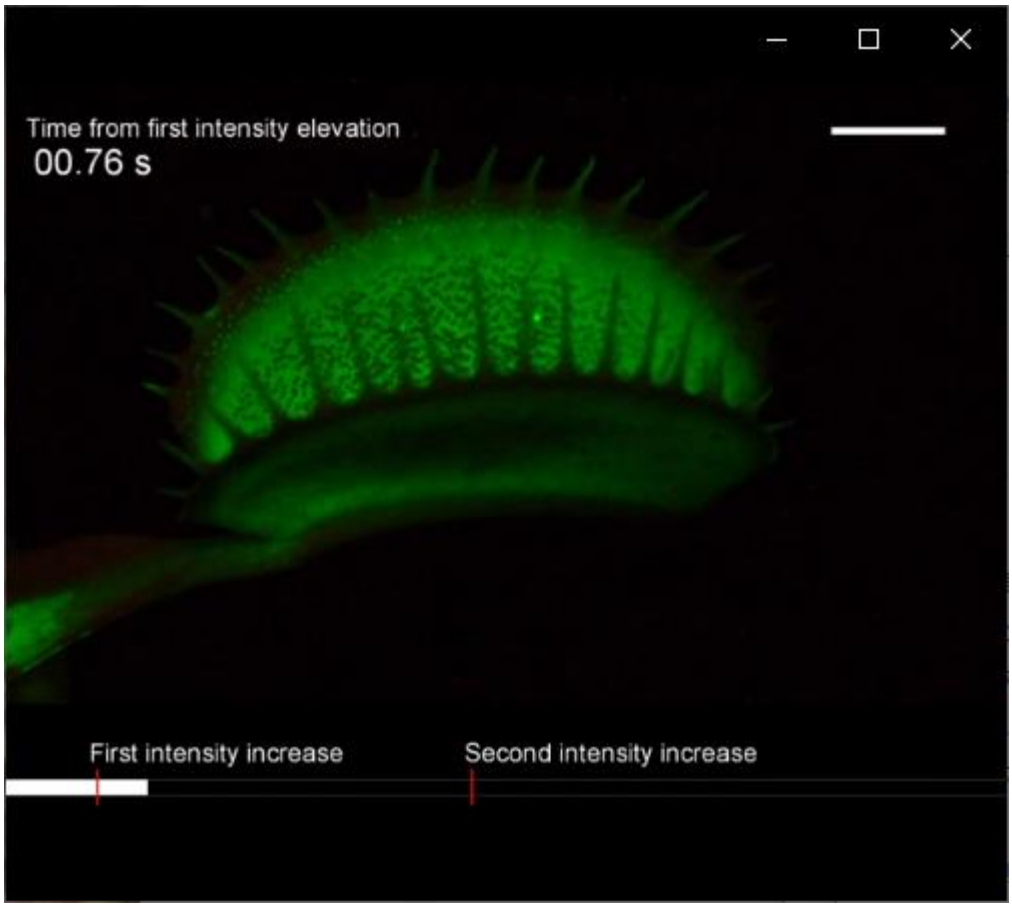

Video 7 | $[Ca^{2+}]_{cyt}$ increases at the leaf immersed the basal part of a petiole in water and leaf closes without mechanical stimulus.

The video is played at real time speed. Time (seconds, s) after the first increase of fluorescence intensity is indicated. Scale bar, 2 mm.
(https://drive.google.com/file/d/1r_dcmht76XVm420Sb7CpdoKTz3tCEYl-/view)

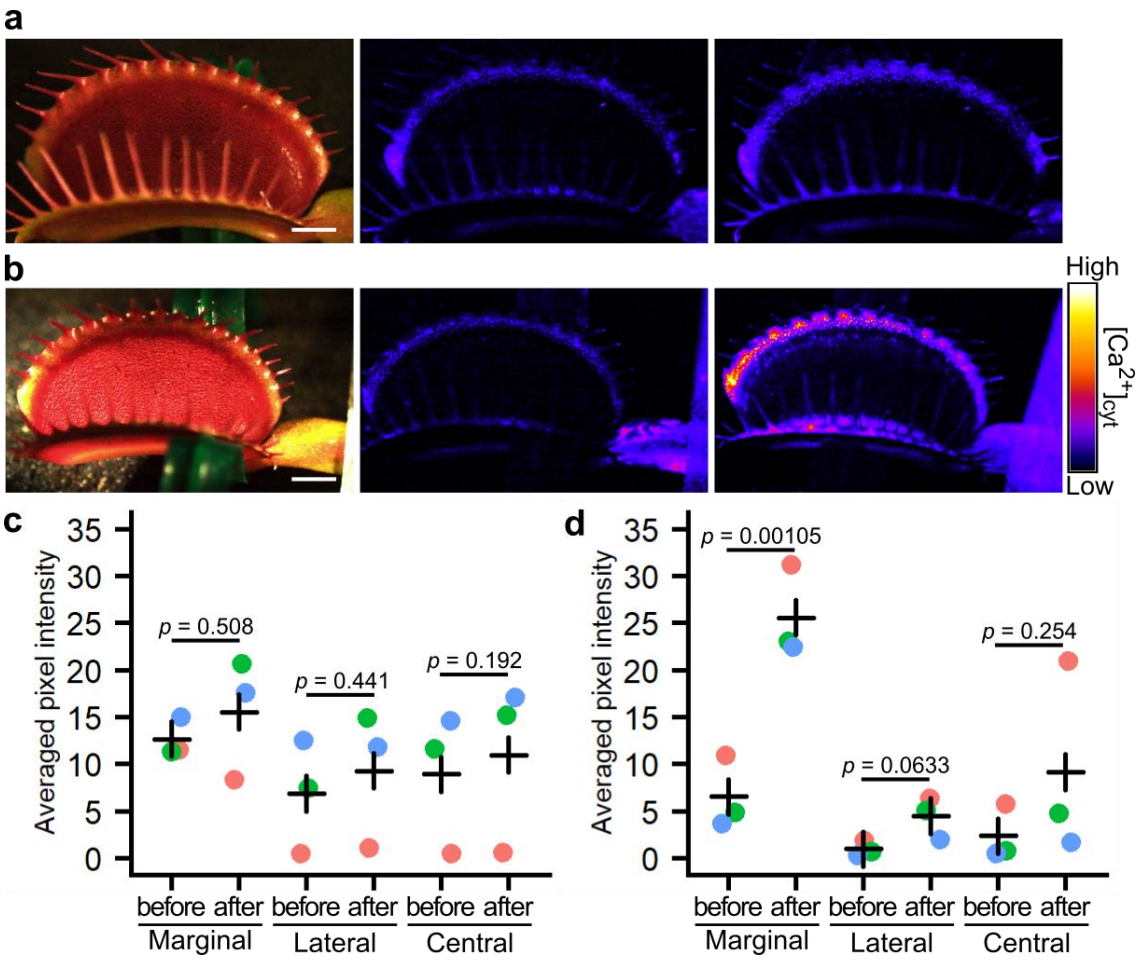

Fig. 19: Immersion in the $LaCl_3$ solution increases fluorescence intensity at the marginal area of leaf blades with no stimuli.

a-b, A bright field image (left) and fluorescence images (others) in adaxial views of GCaMP6f Dionaea leaves before (middle) and 30 minutes after (right) immersion in water (**a**) or 20 mM $LaCl_3$ solution (**b**).

c-d, Averaged pixel intensities at the marginal (Marginal), the lateral (Lateral), and the central areas (Central) of the leaves before and after 30 minutes immersion in water (**c**) (n = 3) or 20 mM $LaCl_3$ solution (**d**) (n = 3). The lateral and the central areas correspond to those shown in Fig. 5h. The marginal area corresponds to the area more lateral to the lateral area. Averaged pixel intensities were calculated as those at lateral and central areas. Paired t test was used to calculate two tail p-values.

Scale bar, 2 mm.

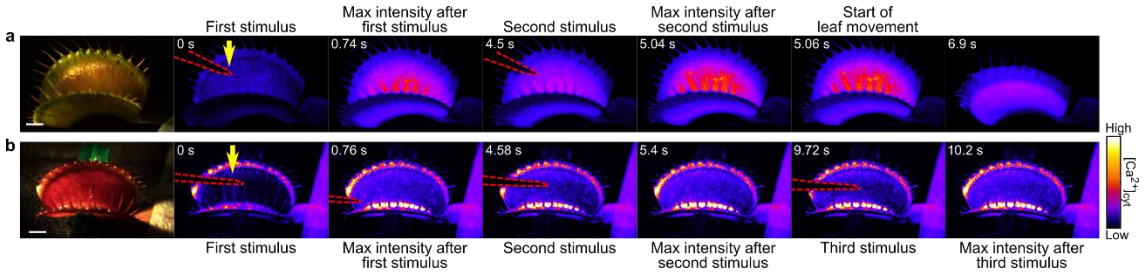

Fig. 20: The $[Ca^{2+}]_{cyt}$ increase induced by mechanical stimuli after immersion of a whole leaf in water or $LaCl_3$ solution.

Bright field images (leftmost) and fluorescence images (others) of GCaMP6f Dionaea leaves after a sensory hair was stimulated with a needle (yellow arrow). Frames are extracted in pseudocolor from those shown in Video 8 (**a**) and Video 9 (**b**). Seconds (s) after the first stimulus are indicated. Red dotted lines indicate the outline of a needle. A leaf was closed by the second stimulus (**a**), but was not by the second and third stimuli (**b**). Max intensity was measured at the whole pictured area. Scale bar, 2 mm.

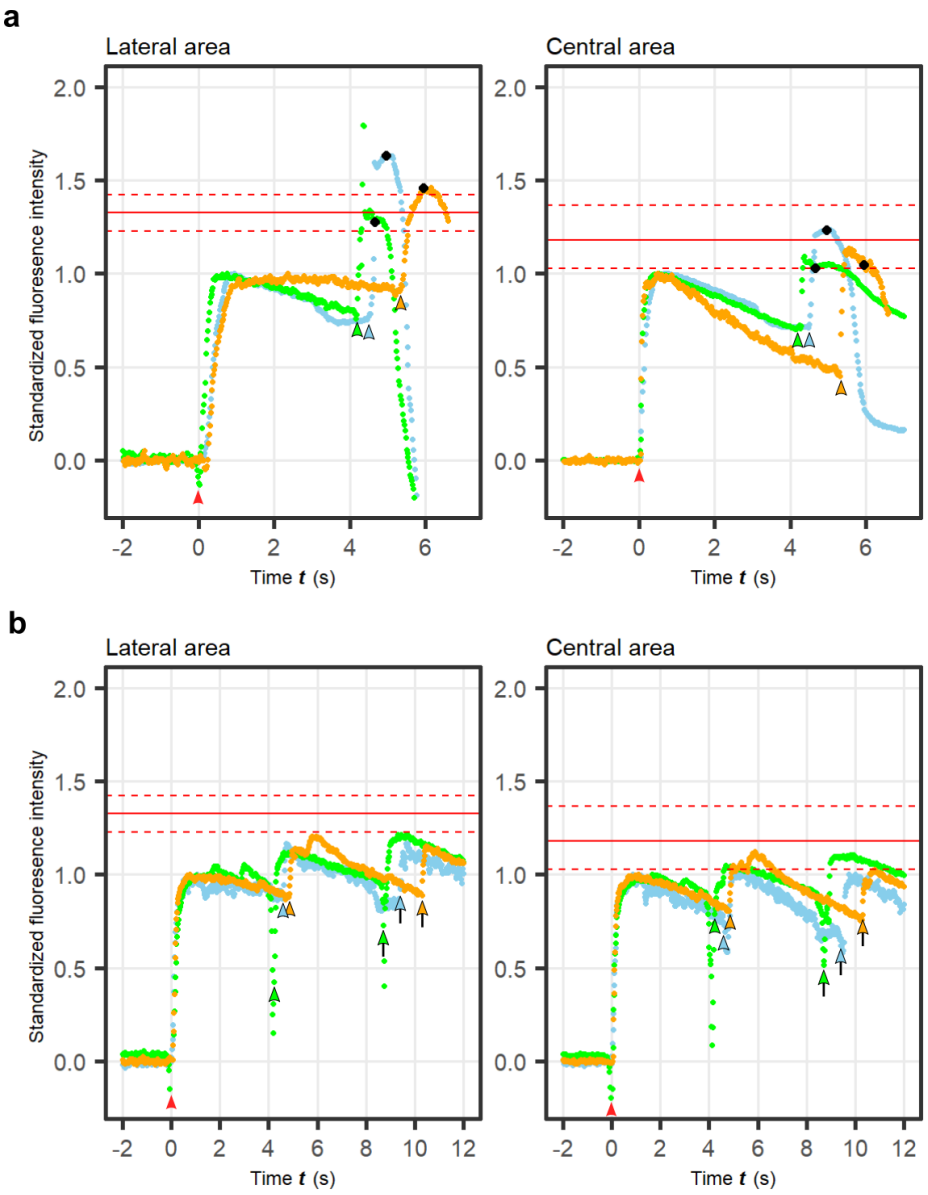

Fig. 21: Temporal fluorescence changes after mechanical stimulation of GCaMP6f Dionaea leaves immersed in the calcium channel blocker $LaCl_3$ solution.

a–b, Representative time courses of the normalized fluorescence intensity at time t [F_t] in the lateral (left) and the central (right) areas 30 minutes after immersion in water (**a**) (n = 3) or 20 mM $LaCl_3$ solution (**b**) (n = 3). Time at the first mechanical stimulus (red arrow-head) is set as 0 second. The second and the third stimuli are indicated by arrow-heads and arrows, respectively. The color of arrow-heads in the second and the third stimuli correspond to that of the plots. Time points when leaf movement started are indicated by black dots. Putative thresholds for the movement (red lines) and their 95% CIs (red dotted lines) are taken from Table 2.

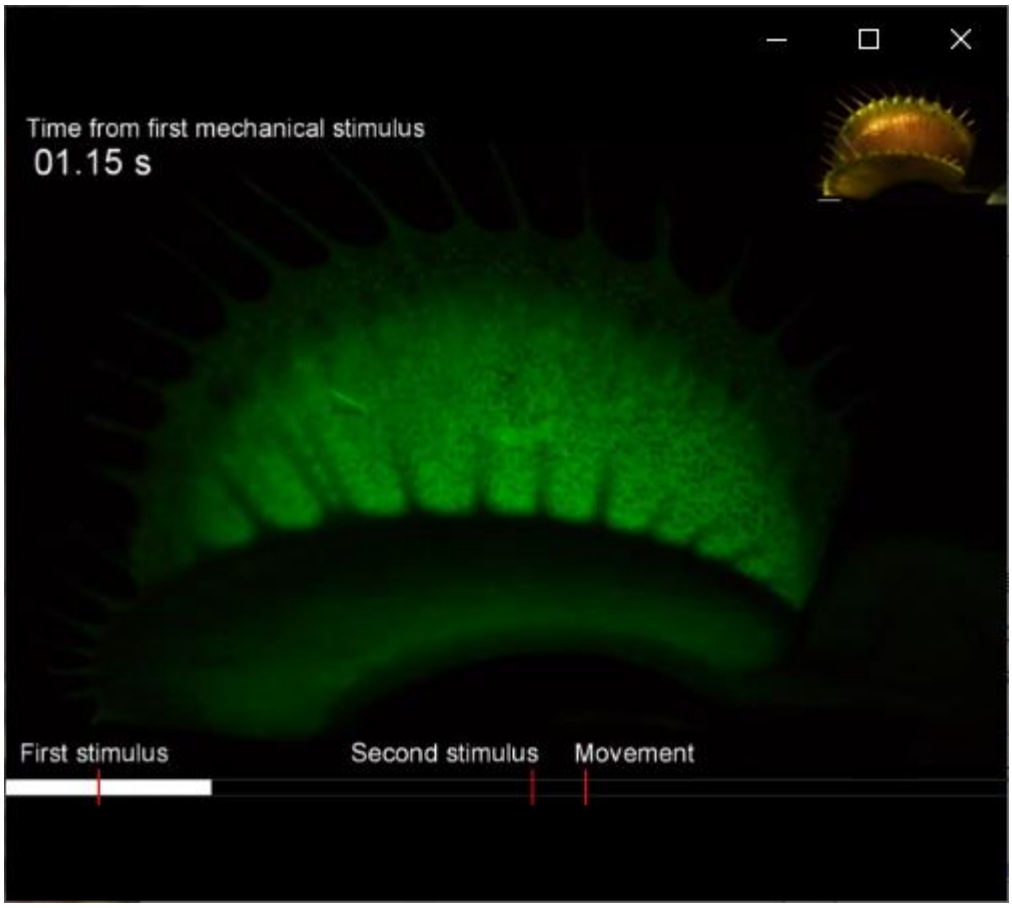

Video 8 | The $[Ca^{2+}]_{cyt}$ increases by successive mechanical stimuli in water immersed leaf as same with untreated leaves.

The video is played at real time speed. Time (seconds, s) after the first mechanical stimulus is indicated. Scale bar, 2 mm.
(https://drive.google.com/file/d/1r_dcmht76XVm420Sb7CpdoKTz3tCEYl-/view)

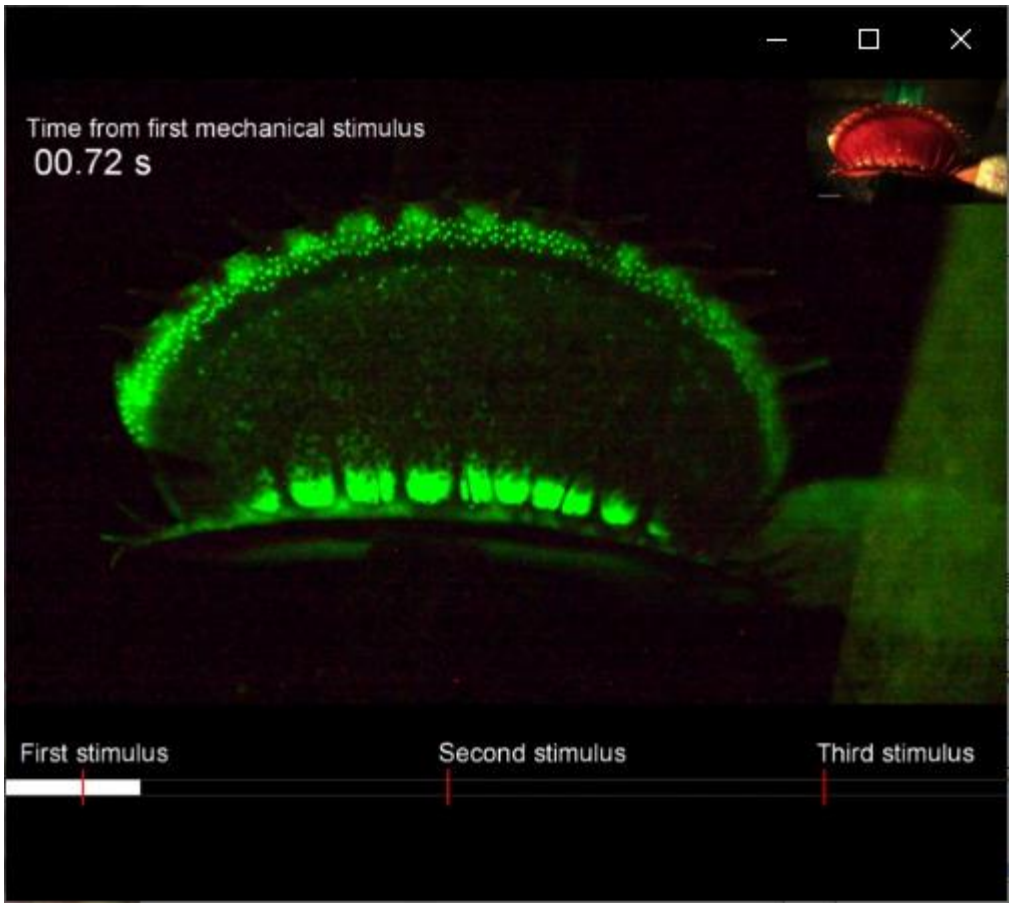

Video 9 | The $[Ca^{2+}]_{cyt}$ increases by first stimulus but not additively increases by second stimulus in $LaCl_3$ solution immersed leaf.

The video is played at real time speed. Time (seconds, s) after the first mechanical stimulus is indicated. Scale bar, 2 mm.
(https://drive.google.com/file/d/1r_dcmht76XVm420Sb7CpdoKTz3tCEYl-/view)

development of the leaf blade and carnivory traits were poorly understood. To define developmental stages, I observed developmental processes with scanning electron microscopy, and defined five stages.

At the stage of leaf primordia, leaves started to convolute at approximately longer than 100 μm in length from leaf apices to leaf bases (Fig. 22a, blue arrow-heads). In this stage, a border between the leaf blade and petiole was indistinguishable. At the same time, primordia of stellate glands developed only at abaxial sides of the leaf primordia (Fig. 22a, yellow arrow-heads). I defined all of these leaf primordia as stage 1.

Subsequently, the margins of the leaf blade and petiole kept protruding except for the border of the blade and petiole (Fig. 22b). This border area eventually became the midrib connecting the leaf blade to the petiole (Fig. 22e, red arrow-head). This stage was defined as stage 2.

After that, the margin of the leaf blade curled inward (Fig. 22c, Fig. 23a, d, g and j), and at the margin, marginal stellate glands emerged at regular intervals (Fig. 23g, red arrow-heads). At this time, the primordia of the sensory hairs appeared on the adaxial side of the leaf blade (Fig. 23d). Also, some of the stellate glands at the abaxial side started to mature (Fig. 22c, yellow arrow-head). I defined this stage as stage 3.

Subsequently, the leaf blade continued to curl inward (Fig. 22c, Fig. 23b, e, h, k and m), and the spaces between the marginal stellate glands started to protrude (Fig. 23k, red arrow-heads). These protrusions eventually formed the teeth (Fig. 23l). At the same time, the digestive glands also started to develop (Fig. 23m). This stage was defined as stage 4.

After the development of glands, sensory hairs, and teeth, the leaf blade opened

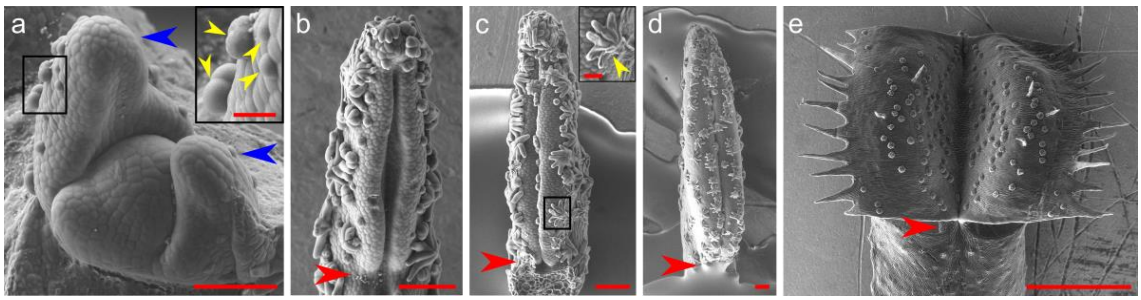

Fig. 22: Development of leaf blades in Dionaea.

Representative shoot apex with leaf primordia (**a**) and developing leaf blades viewed from adaxial sides (**b**-**e**) at stage 1 (**a**), stage 2 (**b**), stage 3 (**c**), stage 4 (**d**) and stage 5 (**e**). Borders between leaf blades and petioles are indicated by red arrow-heads. Of the leaf primordia at stage 1, those that have begun to convolute are indicated by blue arrow-heads. Stellate glands at the abaxial side are indicated by yarrow arrow-heads. Insets of (**a**) and (**c**) correspond to square areas of (**a**) and (**c**). Scale bars, 100 µm in (**a**)-(**c**) and (**d**); 1 mm in (**e**). 25 µm in the insets of (**a**) and (**c**).

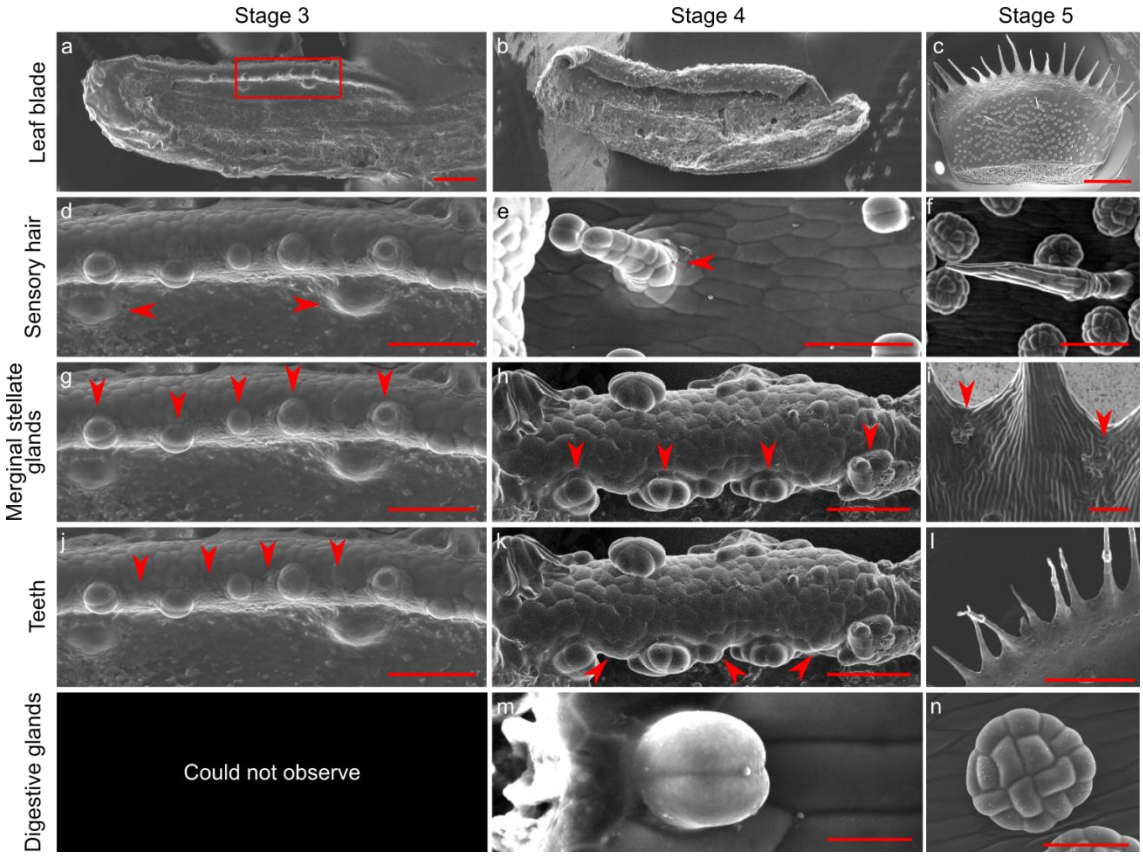

Fig. 23: Development of tissues in Dionaea.

a-c, Representative leaf blades cut by planes perpendicular to the lateral-central axes viewed from adaxial sides at stage 3 (**a**), stage 4 (**b**) and stage 5 (**c**).

d-f, Representative sensory hairs at stage 3 (**d**), stage 4 (**e**) and stage 5 (**f**). Panel (**d**) corresponds to the square area of the panel (**a**). Sensory hair primordia are indicated by red arrow-heads.

g-i, Representative marginal stellate glands at stage 3 (**g**), stage 4 (**h**) and stage 5 (**i**). Panel (**g**) corresponds to the square area of the panel (**a**). Marginal stellate glands are indicated by red arrow-heads.

j-l, Locations where the teeth will be formed (**j**) and representative teeth at stage 4 (**k**) and stage 5 (**l**). Panel (**j**) corresponds to the square area of the panel (**a**). The locations where the teeth will be formed (**j**) and teeth primordia (**k**) are indicated by red arrow-heads.

m-n, Representative digestive glands at stage 4 (**m**) and stage 5 (**n**).

Scale bars, 1mm in (**b**), (**c**) and (**l**); 100 μm in (**a**), (**f**), and (**i**); 50 μm in (**d**), (**e**), (**g**), (**h**), (**j**), (**k**) and (**n**); 10 μm (**m**).

and was defined as stage 5 (Fig. 23c, f, i, l and n).

I sampled leaves and shoot apices at each stage from stage 1 to 5, and performed transcriptome analysis. Further analysis using these transcriptome data will provide candidates of genes related to upstream and downstream pathways of the calcium signaling in Dionaea.

5. Discussion

5.1. Possible mechanisms of memory system using $[Ca^{2+}]_{cyt}$ in Dionaea

My results illuminate how Dionaea achieves signal transduction from sensing of mechanical stimuli towards leaf closure. This study shows that (1) the first mechanical stimulus to a sensory hair increases $[Ca^{2+}]_{cyt}$ in the leaf tissue responsible for movement (Fig. 5), (2) the elevated $[Ca^{2+}]_{cyt}$ decreases exponentially after the first stimulus (Fig. 12d, e and Fig. 14), (3) the second stimulus additively increases $[Ca^{2+}]_{cyt}$ (Fig. 12a and b), and (4) $[Ca^{2+}]_{cyt}$ meets the putative threshold for the movement after the second stimulus (Fig. 12c and Table 2).

These traits of calcium signals are consistent with the traits of the memory system in Dionaea: (1) the first stimulus is memorized in the leaf blade (2) stimulus information is lost in less than 30 seconds (3) the movement is triggered when the second stimulus is added within 30 seconds after the first stimulus. Time courses of the $[Ca^{2+}]_{cyt}$ decay after the first stimulus (Fig. 12d and e), the $[Ca^{2+}]_{cyt}$ threshold for movement (Fig. 12c and Table 2), the leaf movement by the $[Ca^{2+}]_{cyt}$ increase without the mechanical stimulus (Fig. 17 and Fig. 18) and the inhibition of the Ca^{2+} signaling as well as the movement by La^{3+} (Fig. 20 and Fig. 21) are the basis for the memory in Dionaea. Thus, all of my results support the model that the $[Ca^{2+}]_{cyt}$ plays a critical role in not only the rapid movement of the leaf blade but also the hypothesized memory system (Hodick and Sievers, 1988; Hedrich and Neher, 2018).

From my results, two types of models are considerable about the regulation of the movement using the $[Ca^{2+}]_{cyt}$. The first model is that max $[Ca^{2+}]_{cyt}$ after the second stimulus is necessary to trigger the movement. This model is supported by the results that the $[Ca^{2+}]_{cyt}$ additively increased by each mechanical stimulus (Fig. 12a and b), and

there is a threshold of F_{max} to trigger the leaf movement at the lateral region (Fig. 12c and Table 2). In this model, there should be a mechanism to sense the $[Ca^{2+}]_{cyt}$ over a certain threshold but not sense the $[Ca^{2+}]_{cyt}$ under the threshold. The second model is that the $[Ca^{2+}]_{cyt}$ right before the second stimulus is necessary to trigger the movement and the second Ca^{2+} increase is not necessary. This model is supported by the results that the $[Ca^{2+}]_{cyt}$ elevated by the first mechanical stimulus, F_{res} had a threshold to trigger the movement and the decay curve of the elevated $[Ca^{2+}]_{cyt}$ could explain the time limit from the first stimulus to trigger the movement by the second stimulus (Fig. 12c, d, e and Table 2). In this model, the elevated $[Ca^{2+}]_{cyt}$ after the first stimulus changes the downstream signaling pathway, and the second stimulus triggers another signaling pathway that is different from the one triggered by the first stimulus.

Also, there is a possibility that Ca^{2+} indirectly control other downstream molecules. For example, the increase of the $[Ca^{2+}]_{cyt}$ will change electric potential gradients and concentration gradients inside and outside of cells, which passively change ion concentrations through ion channels, and then activate downstream pathway(s).

5.2. Comparison between calcium signal and action potential

My results showed that calcium signals propagate faster in the medial direction (Fig. 8). It has been known that long and large mesophyll cells are arranged in the medial direction (Hodick and Sievers, 1988; Fagerberg and Allain, 1991). This fact suggests that the number of the cell boundaries on the pathways of the calcium signals in medial direction are fewer than those in other directions. Furthermore, if calcium ions diffuse

through the plasmodesmata, the velocities of calcium signals could be explained by the number of cell boundaries in the signal pathway.

This anisotropic differences in propagation velocities and the acceleration of propagation velocities in response to the second stimulus (Fig. 8 and Table 1) are same with the behavior of leaf action potentials (Sibaoka, 1966). However, the calcium signals did not propagate to the marginal area (Fig. 5f) where action potentials propagate (Sibaoka, 1966). There is a possibility that the tissue in the marginal area lacks the function which is required to propagate calcium signal.

All of the action potential, the increase of the $[Ca^{2+}]_{cyt}$ and the leaf movement are inhibited by the calcium channel inhibitor La^{3+} (Hodick and Sievers, 1988) (Fig. 20 and Fig. 21), and still I could not separate action potentials and calcium signals. Therefore, still there is a possibility that both of the Ca^{2+} signal and the movement are parallelly regulated by the action potentials, and the $[Ca^{2+}]_{cyt}$ and the movement have spurious correlation. To investigate this possibility, future genetic studies will be available using the transgenic method in this thesis.

5.3. Further quantitative methods to analyze calcium signaling

In this thesis, I analyzed the relative values of $[Ca^{2+}]_{cyt}$ by standardization based on the hypothesis that thresholds of $[Ca^{2+}]_{cyt}$ to trigger the movements are different between leaves and leaves sense relative differences between the $[Ca^{2+}]_{cyt}$ after the first stimulus and the second stimulus. However, there is also a possibility that leaves sense the absolute $[Ca^{2+}]_{cyt}$. To clarify this point, ratiometric calcium sensors will be useful such as yellow chameleon. After the cold stimuli, glands and venations showed higher fluorescence intensity than other tissues in the leaf blades (Fig. 1c). This result suggests

differences in the amount of $[Ca^{2+}]_{cyt}$ increase or the GCaMP6f expression between tissues. Ratiometric calcium sensor with tissue-specific promoter will also reveal the mechanism of different sensitivity to the stimulus between tissues.

To stimulate sensory hairs mechanically, I tilt the sensory hair until a change in angle was observed under the microscope using a needle, and then released the needle from the sensory hair within 1 second. Although I could not control loading force and degrees of angular displacement to the sensory hairs, sometimes I observed two successive calcium signals and leaf closure when I stimulate one sensory hair slowly only once. This observation is consistent with the result which observed in previous study with measurements of action potentials (Burri et al., 2020). Further analysis by controlling the loading force and degrees of angular displacement of mechanical stimuli will reveal the relationships between stimulation of sensory hairs and calcium signals.

5.4. Further perspectives to analyze thigmonastic movement in Dionaea

My results showed that the $[Ca^{2+}]_{cyt}$ increase triggered by the mechanical stimulus started from the basal part of the stimulated sensory hairs (Fig. 5a and b). By measuring action potentials at sensory hairs, action potentials are not generated without basal parts of the sensory hairs, and it is revealed that the basal part of the sensory hair is the mechano-sensitive tissue (Benolken and Jacobson, 1970). In this tissue, a huge vacuole which is one of the Ca^{2+} storage exists in the cell (Buchen et al., 1983). This vacuole is one of the candidates of Ca^{2+} storage which is used to increase the $[Ca^{2+}]_{cyt}$ in response to the mechanical stimulus. Further analysis with transgenic Dionaea using tissue-

specific or organelle-specific promoters will reveal where Ca^{2+} come from and in which cell layers the $[Ca^{2+}]_{cyt}$ increased.

Immersion of the basal part of the petiole in water triggered $[Ca^{2+}]_{cyt}$ increase at leaf blades, and leaves closed without mechanical stimuli (Fig. 17, Fig. 18 and Video 7). This result suggests that immersion of the basal part of the petiole in water was accepted as a kind of the stimulus in the leaf blade. For example, there are possibilities that cutting of the leaf base was accepted as a wounding stimulus and immersion of the basal part of the petiole in water was accepted as an osmotic stress. Further considerations of the conditions to trigger this artificial movement will give new insights about how Dionaea movement couples with calcium signals.

In addition, since the leaf area with increased $[Ca^{2+}]_{cyt}$ corresponds to the area in which the effective quantum yield of photosystem II, a proxy measure of the proportion of the light absorption by chlorophylls, transiently decreases after the mechanical stimulus to the sensory hair (Pavlovič et al., 2010, 2011) (Fig. 5f and Fig. 11). Previous study proposed that increase of Ca^{2+} in the stroma suppresses reactions in the Calvin cycle (Bulychev and Kamzolkina, 2006), and my results are consistent with this possibility that $[Ca^{2+}]_{cyt}$ increase by the mechanical stimulus suppresses the photosynthesis through the increase of Ca^{2+} concentration also in Dionaea. Studies on the relationships between $[Ca^{2+}]_{cyt}$ dynamics and other physiological responses will give insight on the evolution of carnivory system in plants.

6. General discussion

6.1. Evolution of thigmonastic movement in Dionaea

In this thesis, I showed that the $[Ca^{2+}]_{cyt}$ is increased by the mechanical stimulus, and also this $[Ca^{2+}]_{cyt}$ elevation is necessary to trigger the movement. Recent studies showed that the Ca^{2+} also works as a long-distance signal transmitter in *Arabidopsis thaliana* responding to the wounding stimulus (Toyota et al., 2018). Both caterpillar feeding and leaf-cutting stimulus trigger propagation of the $[Ca^{2+}]_{cyt}$ increase from a cutting site to systemic leaves, which results in the accumulation of a plant hormone jasmonic acid and subsequent defense responses in the systemic leaves.

In carnivorous plants including Dionaea, it has been considered that digestion and absorption-related genes have diverged from defense-responsive genes induced by jasmonic acid (Ruan et al., 2019; Bemm et al., 2016; Palfalvi et al., 2020; Fukushima et al., 2017). For example, expression of jasmonic acid-receptor genes DmJAZ1 and DmCOI1 are upregulated by mechanical stimuli (Böhm et al., 2016), and jasmonic acid and its precursor cis-OPDA also accumulate in the leaf blade after mechanical stimuli (Libiaková et al., 2014). Activation of the jasmonic acid pathways trigger upregulation of the absorption-related genes such as Dionaea ammonium channel DmAMT1 and sodium channel DmHKT1, and also upregulation of digestion-related genes in the digestive fluid such as protease, phosphatase, and chitinase including SENESCENCE-ASSOCIATED GENE 12 (SAG12), SERINE CARBOXYPEPTIDASE-LIKE 49 (SCPL49) and VF chitinase-I (Böhm et al., 2016). Furthermore, gene ontology term enrichment analysis showed that an expression profile of genes responding to the insect capture closely resembles that of genes responding to the insect-feeding and the wounding stimulus in Dionaea. These results support the hypothesis that carnivory-

related genes are duplicated from the defense-responsive jasmonic acid pathway-related genes.

My results showed that the increased $[Ca^{2+}]_{cyt}$ is related to the insect capturing movement in Dionaea as well as the wounding response in *Arabidopsis thaliana*. Thus, the insect-feeding and the wounding responses are candidates for the ancestral characters not only in digestion and absorption but also in the prey capturing function in Dionaea In contrast, my results also showed that the velocities of calcium signaling in response to mechanical and wound stimuli in Dionaea leaf blades are faster than the velocities of calcium signaling in response to wounding stimuli in Dionaea petioles and in response to wounding stimuli in leaf blades and petioles of *Arabidopsis thaliana* (Toyota et al., 2018). These results suggest that Dionaea has acquired a mechanism to propagate calcium signaling at the leaf blade faster than the petiole that *Arabidopsis thaliana* does not have, and this trait is a unique treat not found in the wounding response. Further genetical studies will reveal the origin of the prey capturing system-related genes and its evolution.

6.2. Adaptive significance of the Dionaea memory system

It has been proposed that memory system of Dionaea is adaptive to prevent the movements by the accidental mechanical stimuli such as raindrops or stones (Juniper et al., 1989b). However, it is still a matter of debate because rain drops keep hitting leaf blades while it is raining. My GCaMP6f transgenic Dionaea will be useful to visualize the acceptance of the mechanical stimuli, and to understand the relationships between environmental stimuli and movements.

6.3. Possible regulatory mechanisms of $[Ca^{2+}]_{cyt}$

Ca^{2+} ion is the first observed molecule in this study that is involved in prey capturing in response to the mechanical stimulus. The next questions are how the $[Ca^{2+}]_{cyt}$ increases in response to the mechanical stimulus to a sensory hair and gradually decreases afterward.

Intercellular calcium ion concentration is kept low under normal conditions in the cytosol of plant cells (Hashimoto and Batistic, 2010), and my results indicate that the $[Ca^{2+}]_{cyt}$ decay to the basal level takes longer than the increase in response to the mechanical stimulus. These results suggest possibilities that increase of the $[Ca^{2+}]_{cyt}$ is regulated by a concentration gradient-dependent calcium influx using ion channels, and the intercellular $[Ca^{2+}]_{cyt}$ is decreased by active ion transporters that transport against the concentration gradients. About Ca^{2+} influx, one of the candidate carriers for the Ca^{2+} influx into the cytoplasm is a stimulus-responsive ion channel, such as glutamate like receptor 3.3 (GLR3.3) and GLR3.6, which are able to elevate the $[Ca^{2+}]_{cyt}$ within seconds by using differences of ion concentration between inside and outside of cells (Toyota et al., 2018). It is known that GLUTAMATE RECEPTOR-LIKE family protein is necessary to trigger the $[Ca^{2+}]_{cyt}$ increase in response to the wounding stimulus in *Arabidpsis thaliana* (Toyota et al., 2018). Thus, this gene is a strong candidate that regulates $[Ca^{2+}]_{cyt}$ elevation in Dionaea.

On the other hand, one candidate of the ion transporter involved in the decay of $[Ca^{2+}]_{cyt}$ is Ca^{2+}-ATPase, since ATP concentration decreases after the movement (Williams and Bennett, 1982). However, the prey capturing itself triggers many signaling pathways related to the digestion and the absorption (Bemm et al., 2016), thus also there is a possibility that this ATP consumption is used to activate signaling

pathways that are not related to the Ca^{2+} ejection from the cytosol.

6.4. Candidates of binding targets of Ca^{2+}

After the second stimulus with the increase of the $[Ca^{2+}]_{cyt}$, the leaf movement starts. In this process, the leaf movement finishes within 0.1 seconds (Forterre et al., 2005), suggesting that the Ca^{2+} will trigger the movement without biosynthesis of the molecules. There are both possibilities that the Ca^{2+} directly binds to the downstream molecule or the Ca^{2+} triggers the movement without binding to any other molecules. Examples of Ca^{2+} binding targets are proteins having calcium-binding domains, such as calmodulin proteins with EF-hand motifs, or non-protein molecules, such as pectin which is a calcium-binding polysaccharide. In the case of the calcium-binding protein, the binding of Ca^{2+} changes its conformation, while in the case of pectin, the binding of Ca^{2+} changes its physical properties and increases the mechanical strength of the cell wall. Actin-myosin system is also one of the candidates that Ca^{2+} regulates. In *Mimosa pudica*, it was pointed out that phosphorylation of actin is involved in the thigmonastic movement (Kameyama et al., 2000), and actin-myosin system is known as a regulator of the cytoplasmic streaming which is effected by the Ca^{2+} concentration (Shimmen, 2007). Further analysis using RNA sequencing data in this thesis will provide the candidates of calcium-binding proteins in Dionaea, and those of proteins which regulate non-protein Ca^{2+} binding targets such as pectinase.

6.5. Hypothesized mechanism to trigger the movement in Dionaea

About the movement of Dionaea leaves, it is known that the speed of the movement is enhanced by the elasticity of the leaf blade once after the movement started, thus small power is enough to trigger the movement (Forterre et al., 2005).

However, it is still unknown what mechanism is used to generate the small power to trigger the movement.

Decreasing of turgor pressure is one of the previously hypothesized mechanisms to trigger the movement (Brown, 1916). It has been considered that action potentials trigger efflux of K^+, Cl^-, and water from cells by osmotic pressure in Dionaea and *Aldrovanda vesiculosa* which is the closest relative to Dionaea (Iijima and Sibaoka, 1983; Hedrich and Neher, 2018). Previous studies in other plants suggested that the $[Ca^{2+}]_{cyt}$ elevation is considered as a regulator of the movements at the motor cells of legumes and guard cells by decreasing turgor pressure through the regulations of ion channels (Schroeder and Hagiwara, 1989; Kim et al., 1996; Poppinga et al., 2013). Based on these studies and my results suggest that the decrease of turgor pressure by the $[Ca^{2+}]_{cyt}$ elevation can be one of the possible models to generate power and trigger the movement in Dionaea.

6.6. Conclusion

My transgenic method opened the way to analyze the molecular mechanism of the prey capturing system in Dionaea by a reverse genetical approach. Further studies on the molecular mechanisms of calcium dynamics especially on the relationships of the $[Ca^{2+}]_{cyt}$ change to mechanical stimuli, action potentials, and turgor changes will reveal the mechanisms of the mechano-sensing and the leaf movement, as well as the evolution of the rapid movement in plants by understanding what kind of genes the thigmonasty-related genes are originated from.

7. Acknowledgements

First of all, I really appreciate Professor Mitsuyasu Hasebe for his dedicated supports based on many discussions and advice, I could not proceed with this work without his understanding, deep discussions, and supports. I am grateful to Associate professor Yosuke Tamada for helpful discussions, advice, guidance, and experimental instructions.

I would like to thank the collaborators, Associate professor Masatsugu Toyota for providing the GCaMP6f vector and discussions, Dr. Kenji Fukushima for the establishment of the aseptic culture method of Dionaea and discussions, Dr. Hiroaki Mano for discussions and the optimization of the promoter and terminator of the GCaMP6f vector, Professors Tetsuro Mimura, Izuo Tsutsui and Rainer Hedrich for discussions, and Gergo Palfalvi for transcriptome analysis and discussions.

I thank the Model Plant Research Facility of National Institute for Basic Biology (NIBB) for plant cultivation, the Japan Tobacco Plant Innovation Center for providing pSB11 and LBA4404 harboring pSB1, National BioResource Project (NBRP) for Supplying *Lotus japonicus POLYUBIQUITIN* promoter through Frontier Science Research Center of the University of Miyazaki, Takashi Murata for instructions of microscopy analyses, Hideki Narukawa for instructions of vibratome sections, Yuta Horiuchi and Shoji Segami for instructions of observations using a two-photon microscope, Yoko Matsuzaki for technical assistance, and the members of the Division of Evolutionary Biology and my friends for discussions and supports. Furthermore, I thank my parents and Kaori Houkuwa for understanding my work and encouragements.

8. References

Bemm, F., Becker, D., Larisch, C., Kreuzer, I., Escalante-perez, M., Schulze, W.X., Ankenbrand, M., Weyer, A. Van De, Krol, E., Al-rasheid, K.A., Mithöfer, A., Weber, A.P., Schultz, J., and Hedrich, R. (2016). Venus flytrap carnivorous lifestyle builds on herbivore defense strategies. *Genome Res.*: 1–14.

Benolken, R.M. and Jacobson, S.L. (1970). Response properties of a sensory hair excised from Venus's flytrap. *J. Gen. Physiol.* **56**: 64–82.

Böhm, J., Scherzer, S., Krol, E., Kreuzer, I., Von Meyer, K., Lorey, C., Mueller, T.D., Shabala, L., Monte, I., Solano, R., Al-Rasheid, K.A.S.S., Rennenberg, H., Shabala, S., Neher, E., and Hedrich, R. (2016). The Venus flytrap *Dionaea muscipula* counts prey-induced action potentials to induce sodium uptake. *Curr. Biol.* **26**: 286–295.

Brown, W.H.. and Sharp, L.W.. (1910). The closing response in Dionaea. *Bot. Gaz.* **49**: 290–302.

Brown, W.H. (1916). The mechanism of movement and the duration of the effect of stimulation in the Leaves of Dionaea. *Am. J. Bot.* **3**: 68.

Buchen, B., Hensel, D., and Sievers, A. (1983). Polarity in mechanoreceptor cells of trigger hairs of *Dionaea muscipula* Ellis. *Planta* **158**: 458–468.

Bulychev, A.A. and Kamzolkina, N.A. (2006). Effect of action potential on photosynthesis and spatially distributed H^+ fluxes in cells and chloroplasts of *Chara corallina*. *Russ. J. Plant Physiol.* **53**: 1–9.

Burdon-Sanderson, J. and Page, F. (1876). On the mechanical effects and on the electrical disturbance consequent on excitation of the leaf of *Dionaea muscipula*. **XXV**.

Burri, J.T., Saikia, E., Läubli, N.F., Vogler, H., Wittel, F.K., Rüggeberg, M., Herrmann, H.J., Burgert, I., Nelson, B.J., and Grossniklaus, U. (2020). A single touch can provide sufficient mechanical stimulation to trigger Venus flytrap closure. *PLOS Biol.* **18**: e3000740.

De Candolle, C. (1876). Sur la structure et les mouvements des feuilles du *Dionaea muscipula*. *Arch. Sci. Phys. Nat.* **55**: 400–431.

Chen, T.-W., Wardill, T.J., Sun, Y., Pulver, S.R., Renninger, S.L., Baohan, A., Schreiter, E.R., Kerr, R.A., Orger, M.B., Jayaraman, V., Looger, L.L., Svoboda, K., and Kim, D.S. (2013). Ultrasensitive fluorescent proteins for imaging neuronal activity. *Nature* **499**: 295–300.

Chiu, W., Niwa, Y., Zeng, W., Hirano, T., Kobayashi, H., and Sheen, J. (1996). Engineered GFP as a vital reporter in plants. *Curr. Biol.* **6**: 325–330.

Crisp, P.A., Ganguly, D., Eichten, S.R., Borevitz, J.O., and Pogson, B.J. (2016). Reconsidering plant memory: intersections between stress recovery, RNA turnover, and epigenetics. *Sci. Adv.* **2**: e1501340.

Depicker, A., Stachel, S., Dhaese, P., Zambryski, P., and Goodman, H.M. (1982). Nopaline synthase: transcript mapping and DNA sequence. *J. Mol. Appl. Genet.* **1**: 561–73.

Escalante-Perez, M., Krol, E., Stange, A., Geiger, D., Al-Rasheid, K.A.S., Hause, B., Neher, E., Hedrich, R., Escalante-Pérez, M., Krol, E., Stange, A., Geiger, D., Al-Rasheid, K.A.S., Hause, B., Neher, E., Hedrich, R., Escalante-Perez, M., Krol, E., Stange, A., Geiger, D., Al-Rasheid, K.A.S., Hause, B., Neher, E., Hedrich, R., Escalante-Pérez, M., Krol, E., Stange, A., Geiger, D., Al-Rasheid, K.A.S., Hause, B., Neher, E., and Hedrich, R. (2011). A special pair of phytohormones controls excitability, slow closure, and external stomach formation in the Venus flytrap. *Proc.*

Natl. Acad. Sci. U. S. A. **108**: 15492–15497.

Fagerberg, W.R. and Allain, D. (1991). A Quantitative study of tissue dynamics during closure in the traps of Venus' s flytrap *Dionaea muscipula*. *Am. J. Bot.* **78**: 647–657.

Forterre, Y., Skotheim, J.M., Dumais, J., Mahadevan, L., Dumals, J., and Mahadevan, L. (2005). How the Venus flytrap snaps. *Nature* **433**: 421–425.

Fraustadt, A. (1877). Anatomie der vegetativen organe von *Dionaea muscipula* Ellis. *Cohn Beiträge Biol. der Pflanz.* **2**: 27–64.

Fukushima, K., Fang, X., Alvarez-Ponce, D., Cai, H., Carretero-Paulet, L., Chen, C., Chang, T.H., Farr, K.M., Fujita, T., Hiwatashi, Y., Hoshi, Y., Imai, T., Kasahara, M., Librado, P., Mao, L., Mori, H., Nishiyama, T., Nozawa, M., Pálfalvi, G., Pollard, S.T., Rozas, J., Sánchez-Gracia, A., Sankoff, D., Shibata, T.F., Shigenobu, S., Sumikawa, N., Uzawa, T., Xie, M., Zheng, C., Pollock, D.D., Albert, V.A., Li, S., and Hasebe, M. (2017). Genome of the pitcher plant *Cephalotus* reveals genetic changes associated with carnivory. *Nat. Ecol. Evol.* **1**: 1–9.

Gagliano, M., Renton, M., Depczynski, M., and Mancuso, S. (2014). Experience teaches plants to learn faster and forget slower in environments where it matters. *Oecologia* **175**: 63–72.

Hagihara, T. and Toyota, M. (2020). Mechanical signaling in the sensitive plant *Mimosa pudica* L. *Plants* **9**: 1–10.

Hashimoto, K. and Batistic, O. (2010). Calcium signals : the lead currency of plant information processing. **22**: 541–563.

Hedrich, R. and Neher, E. (2018). Venus flytrap: how an excitable, carnivorous plant works. *Trends Plant Sci.* **23**: 220–234.

Hellens, R., Mullineaux, P., and Klee, H. (2000). Technical focus:a guide to agrobacterium binary Ti vectors. *Trends Plant Sci.* **5**: 446–451.

Hodick, D. and Sievers, A. (1989). On the mechanism of trap closure of Venus flytrap (*Dionaea muscipula* Ellis). *Planta* **179**: 32–42.

Hodick, D. and Sievers, A. (1988). The action potential of *Dionaea muscipula* Ellis. *Planta* **174**: 8–18.

Iijima, T. and Sibaoka, T. (1983). Movements of K^+ during shutting and opening of the trap-lobes in *Aldrovanda vesiculosa*. *Plant cell Physiol.* **24**: 51–60.

J. M. Macfarlane (1892). Contributions to the history of *Dionaea muscipula* Ellis. *Contr. Bot. Lab. Univ. Pennsylvania* **1**: 7–44.

Jensen, M.K., Vogt, J.K., Bressendorff, S., Seguin-Orlando, A., Petersen, M., Sicheritz-Pontén, T., and Mundy, J. (2015). Transcriptome and genome size analysis of the Venus flytrap. *PLoS One* **10**: 1–13.

Juniper, B.B.E., Robins, R.J., and Joel, D.M. (1989). The Carnivorous Plants (Academic Press).

Kameyama, K., Kishi, Y., Yoshimura, M., Kanzawa, N., Sameshima, M., and Tsuchiya, T. (2000). Tyrosine phosphorylation in plant bending. *Nature* **407**: 1997.

Kim, H.Y., Coté, G.G., and Crain, R.C. (1996). Inositol 1,4,5-trisphosphate may mediate closure of K^+ channels by light and darkness in *Samanea saman* motor cells. *Planta* **198**: 279–287.

Knight, H. and Knight, M.R. (2000). Imaging spatial and cellular characteristics of low temperature calcium signature after cold acclimation in *Arabidopsis*. *J. Exp. Bot.* **51**: 1679–1686.

Knight, M.R., Smith, S.M., and Trewavas, A.J. (1992). Wind-induced plant motion

immediately increases cytosolic calcium. *Proc. Natl. Acad. Sci. U. S. A.* **89**: 4967–4971.

Komari, T., Takakura, Y., Ueki, J., Kato, N., Ishida, Y., and Hiei, Y. (2015). Binary vectors and super-binary vectors. In Agrobacterium Protocols (Humana Press: New Jersey), pp. 15–42.

Kurtz, F. (1876). Zur anatomie des blattes der *Dionaea muscipula*. *Arch. Anat., Physiol. Wiss. Med.* **1**: 29.

Libiaková, M., Floková, K., Novák, O., Slováková, L., and Pavlovič, A. (2014). Abundance of cysteine endopeptidase dionain in digestive fluid of Venus flytrap (*Dionaea muscipula* Ellis) is regulated by different stimuli from prey through jasmonates. *PLoS One* **9**: e104424.

Maekawa, T., Kusakabe, M., Shimoda, Y., Sato, S., Tabata, S., Murooka, Y., and Hayashi, M. (2008). Polyubiquitin promoter-based binary vectors for overexpression and gene silencing in *Lotus japonicus*. *Mol. Plant-Microbe Interact.* **21**: 375–382.

Mano, H., Fujii, T., Sumikawa, N., Hiwatashi, Y., and Hasebe, M. (2014). Development of an agrobacterium-mediated stable transformation method for the sensitive plant *Mimosa pudica*. *PLoS One* **9**: 1–11.

Milliken, G.A., Bates, D.M., and Watts, D.G. (1990). Nonlinear regression analysis and its applications. *Technometrics* **32**: 219.

Odell, J.T., Nagy, F., and Chua, N.H. Identification of DNA sequences required for activity of the cauliflower mosaic virus 35S promoter. *Nature* **313**: 810–812.

Palfalvi, G., Hackl, T., Terhoeven, N., Shibata, T.F., Nishiyama, T., Ankenbrand, M., Becker, D., Förster, F., Freund, M., Iosip, A., Kreuzer, I., Saul, F., Kamida, C.,

Fukushima, K., Shigenobu, S., Tamada, Y., Adamec, L., Hoshi, Y., Ueda, K., Winkelmann, T., Fuchs, J., Schubert, I., Schwacke, R., Al-Rasheid, K., Schultz, J., Hasebe, M., and Hedrich, R. (2020). Genomes of the Venus flytrap and close relatives unveil the roots of plant carnivory. *Curr. Biol.* **30**: 2312-2320.e5.

Pavlovič, A., Demko, V., and Hudák, J. (2010). Trap closure and prey retention in Venus flytrap (*Dionaea muscipula*) temporarily reduces photosynthesis and stimulates respiration. *Ann. Bot.* **105**: 37–44.

Pavlovič, A., Jakšová, J., and Novák, O. (2017). Triggering a false alarm: wounding mimics prey capture in the carnivorous Venus flytrap (*Dionaea muscipula*). *New Phytol.* **216**: 927–938.

Pavlovič, A., Slovaková, L., Pandolfi, C., and Mancuso, S. (2011). On the mechanism underlying photosynthetic limitation upon trigger hair irritation in the carnivorous plant Venus flytrap (*Dionaea muscipula* Ellis). *J. Exp. Bot.* **62**: 1991–2000.

Poppinga, S., Masselter, T., and Speck, T. (2013). Faster than their prey: new insights into the rapid movements of active carnivorous plants traps. *BioEssays* **35**: 649–657.

Ruan, J., Zhou, Y., Zhou, M., Yan, J., Khurshid, M., Weng, W., Cheng, J., and Zhang, K. (2019). Jasmonic acid signaling pathway in plants. *Int. J. Mol. Sci.* **20**: 2479.

Sachse, R., Westermeier, A., Mylo, M., Nadasdi, J., Bischoff, M., Speck, T., and Poppinga, S. (2020). Snapping mechanics of the Venus flytrap (*Dionaea muscipula*). *Proc. Natl. Acad. Sci.* **117**: 16035–16042.

Samejima, M. and Sibaoka, T. (1980). Changes in the extracellular ion concentration in the main pulvinus of *Mimosa pudica* during rapid movement and recovery. *Plant Cell Physiol.* **21**: 467–479.

Satter, R.L. and Galston, A.W. (1981). Mechanisms of control of leaf movements. *Annu. Rev. Plant Physiol.* **32**: 83–110.

Schroeder, J.I. and Hagiwara, S. (1989). Cytosolic calcium regulates ion channels in the plasma membrane of *Vicia faba* guard cells. *Nature* **338**: 427–430.

Shimmen, T. (2007). The sliding theory of cytoplasmic streaming: Fifty years of progress. *J. Plant Res.* **120**: 31–43.

Sibaoka, T. (1980). Action potentials and rapid plant movements. In Plant Growth Substances, F. Skoog, ed (Springer-Verlag: Berlin), pp. 462–469.

Sibaoka, T. (1966). Action potentials in plant organs. *Symp. Soc. Exp. Biol.* **20**: 49–73.

Sibaoka, T. (1991). Rapid plant movements triggered by action potentials. *Bot. Mag. Tokyo* **104**: 73–95.

Thellier, M. and Lüttge, U. (2013). Plant memory: a tentative model. *Plant Biol.* **15**: 1–12.

Toriyama, H. (1955). Observational and experimental studies of sensitive plants VI. The development of the tannin vacuole in the motor cell of the pulvinus. *Cytologia (Tokyo).* **20**: 367–377.

Toriyama, H. and Jaffe, M.J. (1972). Migration of calcium and its role in the regulation of seismonasty in the motor cell of *Mimosa pudica* L. *Plant Physiol.* **49**: 72–81.

Toyota, M., Spencer, D., Sawai-Toyota, S., Jiaqi, W., Zhang, T., Koo, A.J., Howe, G.A., and Gilroy, S. (2018). Glutamate triggers long-distance, calcium-based plant defense signaling. *Science.* **361**: 1112–1115.

Vincent, T.R., Canham, J., Toyota, M., Avramova, M., Mugford, S.T., Gilroy, S., Miller, A.J., Hogenhout, S., and Sanders, D. (2017). Real-time in vivo recording of *Arabidopsis* calcium signals during insect feeding using a fluorescent biosensor. *J. Vis. Exp.*: 1–9.

Volkov, A.G. (2019). Signaling in electrical networks of the Venus flytrap (*Dionaea muscipula* Ellis). *Bioelectrochemistry* **125**: 25–32.

Waldron, C., Murphy, E.B., Roberts, J.L., Gustafson, G.D., Armour, S.L., and Malcolm, S.K. (1985). Resistance to hygromycin B - a new marker for plant transformation studies. *Plant Mol. Biol.* **5**: 103–108.

Williams, S.E. and Bennett, A.B. (1982). Leaf closure in the Venus flytrap: an acid growth response. *Science.* **218**: 1120–1122.